NASA Technical Memorandum 85937

N 8 4 - 2 2 5 3 6

# Assessment of Aerodynamic Performance of V/STOL and STOVL Fighter Aircraft

W.P. Nelms

April 1984

# NASA
National Aeronautics and
Space Administration

# Assessment of Aerodynamic Performance of V/STOL and STOVL Fighter Aircraft

W. P. Nelms, Ames Research Center, Moffett Field, California

# NASA

# ASSESSMENT OF AERODYNAMIC PERFORMANCE OF V/STOL AND STOVL FIGHTER AIRCRAFT

W. P. Nelms
NASA Ames Research Center, Moffett Field, California 94035, U.S.A.

## SUMMARY

A summary of the research efforts in the United States to assess the aerodynamic performance of V/STOL and STOVL fighter/attack aircraft is presented. Emphasis will be on research programs at NASA Ames Research Center conducted jointly with the Department of Defense and Industry. Both small- and large-scale research programs are considered when aerodynamic and propulsion/airframe integration activities are discussed. The impact on aerodynamic performance of special configuration features that are related to the V/STOL requirement will be addressed.

## 1. INTRODUCTION

The Navy's desire for increased force dispersal and the possibility of runway denial that confronts the Air Force may dictate the need for V/STOL or STOVL aircraft in the future. Research is now underway in the United States to ensure the readiness of technology for development of this type of aircraft by the late 1990s. The focal point of this research is Ames Research Center, the NASA lead center for powered-lift aircraft. For this reason, this paper emphasizes V/STOL activities at Ames which are conducted jointly with the Department of Defense (DOD) and the Industry.

In particular, aerodynamic performance and propulsion/airframe integration for V/STOL and STOVL fighter aircraft will be addressed. This will include the impact on aerodynamic performance of special configuration features that are related to the V/STOL requirement. The important issues of propulsion systems, handling qualities and control, and ground effects are addressed in other lectures in this series and will not be covered here.

The paper will begin with a brief description of the V/STOL fighter configurations (Ref. 1) which are used in the research programs. Both twin and single engine concepts are considered. For convenience, the presentation will be divided into two parts, beginning with small-scale research programs and concluding with large-scale programs. Subjects that will be discussed in the small-scale area include configuration aerodynamics and propulsion/airframe integration. This latter topic includes in-flight thrust vectoring, top inlet studies, and propulsion simulation in wind-tunnel tests. Large-scale research items addressed are a large-scale twin engine fighter model, high angle-of-attack studies, and thrust augmenting ejector research.

## 2. V/STOL FIGHTER CONCEPTS

A number of V/STOL and STOVL fighter/attack aircraft concepts have been studied in Phase I of a joint NASA Ames/Navy/Industry research program. These concepts have been described in a previous lecture (Ref. 1) which includes both twin and single engine configurations. Several small- and large-scale wind-tunnel models of these aircraft concepts have been fabricated and used in the research programs to assess aerodynamic performance. These models are representative of the actual aircraft defined in detailed systems studies and therefore go beyond "generic research models," since many of the uncertainties are configuration dependent. The objective is to develop an aerodynamic data base on a number of promising concepts and to ensure the readiness of technology for development of this type of aircraft. The following paragraphs give a brief review of the twin and single engine aircraft concepts.

The twin-engine concepts are shown in Fig. 1 and are described in Ref. 1. Additional information on these concepts is given in Refs. 2-7. A design (Refs. 1-3) by General Dynamics (E205) is shown at upper left in Fig. 1. Lift augmenting ejectors of the short-diffuser type (Alperin) are used for propulsive lift. These are located in four bays that are inboard of the engine nacelles. The design also features a vectored engine over the wing (VEO) lift improvement concept, strakes inboard of the nacelles, a canard, and a single vertical tail. At the upper right of Fig. 1, a design by Grumman is illustrated (Refs. 1, 2, and 4). This concept features a General Electric Remote Augmented Lift System (RALS) for propulsive lift (Ref. 1). Two aft-mounted General Electric Augmented Deflector Exhaust Nozzles (ADEN) (Ref. 1) at the wing trailing edge and dual forward burner/nozzles compose this propulsive lift system. A concept by Northrop is shown at lower left (Refs. 1, 2, and 5). Northrop also uses a RALS with two aft ADEN nozzles and a single burner/forward nozzle. This concept features two large wing-mounted afterbodies to provide internal volume for fuel, avionics and landing gear stowage, and to provide a mounting for the twin vertical tails. The additional internal volume is needed because of space requirements of the propulsive lift system.

The three concepts described are horizontal attitude takeoff and landing (HATOL) aircraft. The next two use a vertical attitude takeoff and landing (VATOL) scheme, or commonly referred to as "tail sitters." The lower center concept shown in Fig. 1 is another design by Northrop (Refs. 1, 2, and 6). Two turbojet engines with swiveling nozzles are used for propulsive lift while the aircraft is in the vertical attitude. This is a tailless design with wing leading edge extensions (LEX) and a top-mounted inlet system. The final concept at lower right of Fig. 1 is a configuration by Vought (Refs. 1, 2, and 7). Again, swiveling nozzles are used for vertical flight. Vought has used a side-mounted inlet design with canards. It should be noted that both VATOL concepts also have conventional/short takeoff and landing capability as depicted by the Vought design with an overload of stores.

The single engine concepts studied in Phase I of the joint Ames/Navy/Industry program are shown in Fig. 2. These were discussed in the previous lecture (Ref. 1) and are described in detail in Refs. 8-13. A design by General Dynamics (E7) is shown at upper left (Refs. 1, 8-10). Two thrust augmenting ejectors located longitudinally on each side of the fuselage in the wing root area provide the forward lift while a deflecting two-dimensional nozzle located on the underside of the fuselage provides the aft lift. The engine fan flow feeds the ejectors and the engine core flow is exited through the deflecting nozzle while in vertical flight. For forward flight, the ejectors are shut down and the fan flow exits through the aft axisymmetric nozzle. The core flow continues to be exhausted through the two-dimensional nozzle. This concept is a tailless design

that has the F16 forward fuselage and vertical tail. A design by Rockwell (Refs. 1, 8, and 11) is shown at the upper right of Fig. 2. This concept features spanwise-lift augmenting ejectors both forward and aft on the wing for propulsive lift. An alternate design has a forward ejector system that is rotated to a chordwise position. Both designs are tailless configurations with top-mounted inlet systems.

A "four-poster" concept developed by McDonnell Douglas is shown at the lower left of Fig. 2 (Refs. 1, 8, and 12). This concept uses a deflected thrust propulsive lift system with fan stream burning and it includes features such as side-mounted inlets and a canard. Finally, a concept developed by Vought is shown at lower right of Fig. 2 (Refs. 1, 8, and 13). A tandem fan propulsion system is used to provide propulsive lift in this highly integrated wing-canard design. This concept features a high degree of wing/body blending and the use of multiple control surfaces including forward ventral surfaces with two-axes of travel.

## 3. SMALL-SCALE RESEARCH

Research activities involving the use of small-scale models in both low- and high-speed wind tunnels is described. Generally, small-scale testing is conducted first to sort out any major configuration problems before large-scale models are constructed. Small-scale model research addresses two subjects that are closely related — configuration aerodynamics and airframe/propulsion integration.

### 3.1 Configuration Aerodynamics

The uncertainties that affect aerodynamic performance for the previously mentioned V/STOL fighter concepts will be described. The uncertainties associated with configuration characteristics driven by propulsive lift requirements will be emphasized. Next, the wind-tunnel models and tests will be described and then example results will be given.

### 3.1.1 Aerodynamic Uncertainties

In any new aircraft system, there are uncertainties in such discipline areas as propulsion, aerodynamics, structures, and avionics. For example, experience indicates that in the early phases of development, V/STOL aircraft are likely to exhibit stability, control, and flying-quality uncertainties in the takeoff/landing, hover, and transitional modes of flight. Ground effects such as suckdown and recirculation are important areas of concern. Operating from small, heaving ships in poor weather conditions will most assuredly present problems. There are uncertainties that relate to new propulsive lift concepts that must be explored. In other words, research is needed in many of the technical areas that are related to V/STOL aircraft development; however, the emphasis here is on identification of the uncertainties in aerodynamics. In particular, aerodynamic performance in the up-and-away flight mode will be emphasized in the section on configuration aerodynamics.

Therefore, a number of uncertainties that affect aerodynamic performance have been identified for each of the twin and single engine V/STOL fighter concepts in the joint Ames/Navy/Industry research program. These are briefly summarized in Figs. 3 through 11 for each of the concepts. Obviously there are many uncertainties that are common to all concepts and there are some that apply not only to V/STOL, but to CTOL aircraft as well. Those uncertainties that are uniquely associated with the V/STOL requirement are highlighted here.

General Dynamics. The General Dynamics' twin engine design is dictated by the incorporation of thrust augmenting ejectors for propulsive lift in the thick regions inboard of the nacelles. This results in an unusual wide-body type of configuration that is totally different from existing aircraft. The minimum drag, and particularly the supersonic wave drag, is of concern because of the large volumes required for the vertical lift system (Fig. 3). In other words, is this a reasonable transonic/supersonic fighter configuration and can the drag levels be predicted for this wide-body concept using existing methods?

Integration of the forward ejector bays, the outboard nacelles, and the canards results in a conceptual design that has a large amount of planform area that is located well forward on the aircraft. The question arises as to where the aerodynamic center is located for this type of configuration and its travel with Mach number. Can the design be configured with subsonic instability that is acceptable for a post-1995 fighter aircraft? Also, can existing techniques adequately predict the aerodynamic center location for this type of wide-body design?

For a maneuvering fighter aircraft, the maximum usable lift and the onset of wing buffeting are important considerations; both are uncertain for this type of configuration. The lateral-directional characteristics are uncertain for this unique wide-body concept since both the experimental data and the adequate prediction methods are lacking.

Grumman. In the Grumman RALS twin engine design we see a similar concern for minimum drag and, in particular, transonic wave drag that is associated with the added volume that is required by the propulsive lift system (Fig. 4). Again, there is an uncertainty of the aerodynamic performance that is associated with the unusual wide-body configuration.

Northrop (HATOL). The Northrop RALS twin engine design also shares the minimum drag and transonic wave drag uncertainties that are associated with the added propulsive lift system volume (Fig. 5). In this configuration, Northrop has attempted to gain back internal volume that is lost to the propulsive lift system by adding wing-mounted afterbodies. However, it is not clear whether these relatively large-volume bodies can be integrated into a reasonable transonic fighter configuration without undue drag penalties. If they can, this offers the designer many desirable options. Finally in the Northrop concept, the concern of the canard/ wing interactions is evident; this applies to the prior two concepts as well. There are two reasons the canard is used on these propulsive lift concepts: one is to trim out the aft-deflected thrust with a positive-lift producing canard deflection; another is to improve the high angle-of-attack aerodynamic performance.

Northrop (VATOL). The Northrop twin-engine VATOL concept also has the concerns for transonic wave drag and aerodynamic center travel with Mach number (Fig. 6). In addition, this concept depends on the wing

leading-edge extension (LEX) for good high-angle-of-attack performance. The LEX affects the longitudinal aerodynamics, the vertical tail effectiveness, and the flow quality to the top-mounted inlet on this concept. Top-mounted inlets offer many advantages to V/STOL fighter aircraft. Reduced radar cross section and a clear undersurface for mounting stores and for easier mating to the arresting device, are advantages to this particular VATOL concept. A potential and significant advantage of top-mounted inlets to HATOL configurations is reduced ingestion of hot gases and debris during takeoff and landing. However, the effect of the airframe on this type of inlet system is of concern, particularly at the angles of attack for maneuvering.

Vought. Finally, the Vought twin-engine VATOL design exhibits many of the uncertainties already mentioned including minimum drag, wing/canard interactions, and buffet onset (Fig. 7).

Turning to the single engine concepts, a number of uncertainties that affect the aerodynamic performance of these aircraft have been identified in the joint Ames/Navy/Industry program.

General Dynamics. When the General Dynamics single engine design is considered, a number of the uncertainties that are a direct result of the requirements for propulsive lift are seen (see Fig. 8). There is a concern for minimum and transonic wave drag. Another concern is the large, forward fuselage vertical surface that forms the inboard ejector diffuser surface because of its effect on the lateral/directional stability of the configuration. This large, slab-sided area forward of the aircraft center of gravity is potentially destabilizing. Another concern is the limitation to the optimum wing design that is imposed by the necessity to incorporate the ejector lift system into the wing root area. Finally, the unique integration of the two-dimensional core nozzle with the underside of the fuselage creates an uncertainty in afterbody drag.

Rockwell. The successful incorporation of the spanwise-thrust augmenting ejector system into the wing is a major concern of the Rockwell single-engine concept (Fig. 9). The alternate configuration, in which the forward ejector is rotated 90°, may be a better design. In any event, the minimum drag of this concept is of concern because of the volume requirements of the propulsive-lift system. The top inlet uncertainties on this concept reaffirms the need for technology studies in these types of inlet systems. The uncertainty that is involved in the prediction of the aerodynamic performance of this design at high angle of attack applies to all of the concepts.

McDonnell Douglas. The deflected thrust propulsive lift concept used by McAir in their single engine V/STOL fighter design resulted in the use of a canard. This close-couple canard is responsible for some of the uncertainties (Fig. 10). The canard contribution to high angle-of-attack lateral/directional instability is a concern. Generally, close-coupled canards, especially with dihedral, tend to reduce directional stability which leads to a larger vertical tail. However, these effects are dependent on canard location and the location and type of vertical tail (single or twin tail). The reduction in longitudinal stability that is caused by the canard is a concern, but the addition of a horizontal tail could improve this situation. The three surface design is an option on this concept. Existing analytical and empirical techniques generally cannot be used to predict these canard effects accurately, because they are very configuration-dependent as a result of the aerodynamic interaction between the canard, the wing, and the other aircraft surfaces.

The deflected-thrust propulsive lift concept leads to other uncertainties, one of which includes the effect of large half-axisymmetric inlets on lateral/directional stability. Another uncertainty includes the nonlinearities in pitching moment characteristics that are caused by the forward location of the propulsion system. This engine location can also have an effect on the configuration drag. In fact, a major unknown on this concept is the subsonic and supersonic minimum drag. In addition, the propulsive flow effects on the aerodynamic performance of this design is an uncertainty, particularly at transonic speeds where the concern is the effect on drag. Also, the jet plume interference effect on the downstream aircraft surfaces is an unknown factor for this deflected-thrust concept.

Vought. The uncertainties of the Vought single engine, tandem fan design are outlined in Fig. 11. The aerodynamic performance of this concept is highly affected by the close-coupled canard in the wing plane, the highly swept strakes, and the high degree of wing/body blending. These characteristics combine to produce uncertainty in both the longitudinal and lateral/directional aerodynamics, particularly at the higher angles of attack. These same configuration features make available prediction methods questionable. Effectiveness of the multiple control surfaces on this design is uncertain, particularly the capability of the forward ventral surface with two-axes of travel in producing direct lift and direct side force. Finally, the minimum drag associated with the configuration volume for the tandem fan propulsion system is uncertain.

3.1.2 Wind Tunnel Models and Tests

Several of the contractors from Phase I of the joint NASA Ames/Navy/Industry research program were selected to fabricate wind-tunnel models in Phase II. These models are used to assess the aerodynamic performance and to investigate the aerodynamic uncertainties for the concepts from Phase I. Both twin- and single-engine models are included. These models are briefly described in this section together with a few comments about the wind-tunnel tests.

3.1.2.1 Twin-Engine Models

General Dynamics. In Phase II, General Dynamics built a wind-tunnel model to simulate the up-and-away flight configuration of their twin-engine design using thrust augmenting ejectors for propulsive lift (Configuration E205). This 9.4% scale model, which is sized for testing in the Ames Unitary and 12-Foot Wind Tunnels, is shown in Figs. 12 and 13. The model is built of high-strength steel to withstand the loads that are associated with high-angle-of-attack testing at transonic Mach numbers. It is a large model for testing at these speeds, and has a span of 1.07 m (42.01 in.) and a length of 1.57 m (61.86 in.). Additional dimensional data for the model are presented in Table 1.

This versatile model provides the following features: (1) variable wing leading-edge and trailing-edge flaps; (2) variable incidence canard with variable leading-edge and trailing-edge flaps; (3) variable longitudinal canard location; (4) alternative inboard strake shapes; (5) all-movable vertical tail; (6) wing-root bending moment gage; and (7) the ability for testing component buildup. The model has flow-through nacelles,

and the internal drag of these nacelles is determined during the tests using a precalibrated 20-tube rake mounted at the exit of each duct. A 6.25-cm (2.5-in.) high-capacity, six-component Task balance is sting-mounted internally in the model to measure the aerodynamic forces.

Northrop (HATOL). The 9.5% scale model fabricated by Northrop to simulate their twin-engine RALS concept is shown in Figs. 14 and 15. The model is sized for testing in the Ames Unitary and 12-Foot Wind Tunnels, and it has been designed to withstand the loads that are encountered at high angles of attack at transonic speeds. As is the case with the General Dynamics model previously described, the Northrop model is relatively large for testing at transonic-supersonic speeds. The HATOL model has a span of 0.95 m (37.14 in.) and an overall length of 1.52 m (59.84 in.). Table 2 gives additional dimensional data.

The following features are available on the model: (1) variable wing leading-edge and trailing-edge flaps, (2) variable incidence canard, (3) all-movable vertical tails, and (4) the ability for testing component buildup.

Northrop (VATOL). For Phase II, Northrop built a 9.5% scale model of their twin-engine VATOL configuration shown in Figs. 16 and 17. The model, which is sized for testing at subsonic through supersonic speeds in the Ames Unitary and 12-Foot Wind Tunnels, has been designed to withstand the loads at high angle of attack at transonic speeds. It has a 0.95-m (37.14-in.) span and an overall length of 1.50 m (58.91 in.). Additional dimensional data for the VATOL model are given in Table 3.

The Northrop model has the following features: (1) variable wing leading-edge and trailing-edge flaps, (2) alternative LEX size and LEX-off capability, (3) all-movable vertical tail, and (4) the ability for testing component buildup. In addition, each duct had 22 total pressure tubes and four static pressure orifices that are permanently mounted internally near the inlet throat to obtain initial data on the effects of the air-frame on the top-mounted inlet system. A precalibrated, 21-tube rake at the exit of each flow-through duct is used to determine the internal drag during the tests. A 5.08-cm (2-in.), high-capacity, six-component Task balance is sting-mounted internally in the model to measure the aerodynamic forces.

3.1.2.2 Single-Engine Models

General Dynamics. In Phase II, General Dynamics fabricated a wind-tunnel model to simulate the up-and-away flight configuration of their single-engine design which featured a combination of augmenting ejector/thrust deflection for propulsive lift (Configuration E7). This 11.1% scale model sized for testing in the Ames 11-Foot, 9- by 7-Foot, and 12-Foot Wind Tunnels is shown in Figs. 18 and 19. The model is constructed of high-strength steel to withstand the loads that are associated with high angle-of-attack testing at transonic speeds. This is a very large model for testing at these speeds. It has a wing reference area of 0.72 m$^2$ (7.79 ft$^2$), a span of 1.10 m (3.6 ft), and a length of 1.59 m (5.23 ft). Additional dimensional data for the model is given in Table 4.

This model has the following features: (1) a baseline wing with camber and twist and an alternate "plain" wing (no twist and camber), (2) variable trailing-edge flaps, (3) deflectable rudder, (4) missiles mounted on the wing tips or beneath the wings, (5) wing tip extensions, (6) wing-root bending moment gage and wing-tip accelerometer, and (7) the ability for testing component buildup. The model has a flow-through inlet system. The internal drag of this system is measured during the tests using two precalibrated rakes with total and static pressures — one rake at the exit of the two-dimensional nozzle and the other rake at the axisymmetric nozzle exit. A 6.35-cm (2.5-in.) high-capacity, six-component Task balance is sting-mounted internally in the model to measure the forces.

McDonnell Douglas. McDonnell Douglas (McAir) designed and fabricated a 9.2% scale wind-tunnel model of their deflected-thrust concept (configuration 279-3). The model (Fig. 20) is sized for testing in the Ames Unitary and 12-Foot Wind Tunnels. High-strength steel is used in the model construction to withstand high-angle-of-attack testing in these facilities. This versatile model can be tested in both a flow-through and a jet-effects mode. Figure 21 shows the flow through configuration which is supported by a sting that exits through the aft fuselage. The jet effects model is supported through the vertical tail. The model has a 1.01-m (3.30-ft) span and a length of 1.55 m (5.08 ft). Table 5 gives additional model information.

The following features are provided in this model: (1) variable wing leading-edge and trailing-edge flaps, (2) a remotely actuated, variable incidence canard, (3) two longitudinal wing locations, (4) a horizontal tail which allows three-surface testing, as well as canard- or aft-tail-alone testing, (5) deflectable rudder, (6) wing-root bending moment gage and wing-tip accelerometer, and (7) the ability for testing component buildup. On the flow-through model, the internal drag is measured during the tests by precalibrated rakes permanently mounted in the ducts. A 6.35-cm (2.5-in.) high-capacity, six-component Task balance is sting-mounted internally in the model to measure the aerodynamic forces.

On the jet-effects model, both cruise and fan-stream burning nozzle settings can be tested using high pressure air. A number of other items have been added to this jet effects model including (1) static pressure taps on the aft fuselage, at the wing root, and on the thermal ramps, (2) total pressure rakes for surveying the plume, and (3) additional nozzle ramp spacers to allow a parametric study of wake distance from the fuselage. In addition, a number of "dummy" sting components are available to allow determination of sting and sting-shroud interference during testing of the flow-through and jet-effects models.

3.1.2.3 Wind-Tunnel Tests

Tests of the twin- and single-engine V/STOL fighter models are primarily conducted in three Ames major facilities — the 11-Foot Transonic, the 9- by 7-Foot Supersonic, and the 12-Foot Pressure Wind Tunnels. (Northrop has also tested its twin-engine models and General Dynamics its single-engine model in their own 7- by 10-foot wind tunnels.) The tests in the Ames tunnels cover an overall Mach number range from 0.2 to 2.0 at a constant Reynolds number of 9.84 × 10$^6$/m (3.0 × 10$^6$/ft). Excursions in Reynolds number are made to determine the effect of this parameter at several Mach numbers.

In the 12-Foot Pressure Wind Tunnel, tests are conducted at Mach 0.2 and 0.4. Angle of attack is varied to 85° on a two segment support system, the first from approximately -5° to 45° and the second from approximately 35° to 85°. Angle of sideslip is varied from about -5° to 10°.

In the 11-Foot Transonic Wind Tunnel, the Mach number is continuously variable from 0.4 to 1.4. Angle of attack is varied from approximately -5° to 28°, and angle of sideslip from -4° to 10°. In the 9- by 7-Foot Supersonic Wind Tunnel, the Mach number range of 1.5 to 2.0 is covered in tests of these models with some excursions to Mach 2.5 for some configurations. Angle of attack is varied from -5° to 15° and angle of sideslip from -4° to 8°.

### 3.1.2.4 Test Plans

To date, the three twin-engine models have been tested in all three tunnels, and most of the results have been analyzed and reported. Extensive tests of the two single-engine models are planned for 1984 and 1985.

A number of other test activities are planned that relate to the General Dynamics E7 design. In addition to the above described one-ninth-scale force model tests, NASA Lewis has tested a one-third-scale, one-half-span model to study the ejector performance. (This will be described later in the ejector research section.) This model has now been converted by General Dynamics to a full-span powered model with a flowing inlet. Tests of this model are planned in the NASA Langley 4- by 7-Meter Tunnel to study the aircraft's transition characteristics. Also in progress is the construction of a 0.15-scale powered free-flight model to be tested at the NASA Langley 30- by 60-Foot Wind Tunnel in the summer of 1984. This test will begin to determine the control laws for the E7-flight-control system. A number of large-scale activities are also planned.

### 3.1.3 Example Results

A number of uncertainties that affect aerodynamic performance and are attributable to configuration features that relate to the V/STOL requirement have been identified. Many of these uncertainties have been investigated in the wind-tunnel test program just discussed. A few examples of the results from this test program that relate to these uncertainties will be briefly described. Again the discussion will be limited to the up-and-away flight mode. The results presented are taken from Refs. 14 through 22.

### 3.1.3.1 Minimum Drag

Among the major uncertainties that are associated with the V/STOL requirements for these future fighter aircraft are the minimum drag and transonic wave drag. These effects on aerodynamic performance were identified as concerns by all of the contractors in the present research program. The uncertainties are a result of the additional volume and surface area requirements associated with the propulsive lift system as compared to conventional takeoff and landing (CTOL) fighter aircraft. In addition, the ability to predict these drag characteristics for these unique configurations using existing techniques is a major uncertainty.

The minimum drag coefficients of the three twin-engine models versus Mach number are shown in Fig. 22. These are presented for a wind-tunnel test Reynolds number of $3 \times 10^6$/ft and are based upon the wing reference area of the respective models. A number of observations can be made about these data.

The minimum drag for these unusual types of configurations are predicted reasonably well at subsonic speeds. However, at supersonic speeds the minimum drag is both over and underpredicted on the General Dynamics and Northrop VATOL models (Refs. 16 and 21). Thus the experimental data base for these kinds of configurations shows the research needed to improve the prediction methods.

How do these drag characteristics compare to existing fighter aircraft? The subsonic minimum drag for several high-performance CTOL fighters is in the vicinity of a drag coefficient (CD) of 0.0200 (200 counts), and the supersonic drag level varies between 400 and 500 counts. Therefore, despite the additional volume and wetted area required for the propulsive lift system, these V/STOL configurations appear to have reasonable drag levels. In fact, the two Northrop designs appear to be on the low side, particularly at supersonic speeds.

The drag coefficients that are presented in Fig. 22 are based on the planform area of the wing with its leading and trailing edges extended to the fuselage centerline, a standard way of defining reference area. However, as noted in Ref. 19, this definition of reference area can lead to difficulties when comparing configurations which have much of their lift generated by surfaces other than the wings (canards, strakes, etc.). A more reasonable reference area has been found to be the total configuration planform area (Fig. 23 taken from Ref. 19). Here the lift curve for the E205 ejector configuration is apparently far superior to the Northrop HATOL and VATOL designs (left of figure), but essentially collapses onto the HATOL and VATOL curves when the total planform area is used (right of figure). The Northrop curves have also been reduced, but to a lesser degree. If these same area ratios are applied to the minimum drag data of Fig. 22, the resulting revised drag levels would be the ones that are shown in Fig. 24. On this basis, the differences in the minimum drag coefficients of the configurations are reduced, although the HATOL and VATOL supersonic levels are still lower. In fact, the experimental minimum drag of the Northrop HATOL design is worthy of note.

In an effort to gain additional internal volume to offset that lost to the propulsive lift system, Northrop uses two wing mounted afterbodies on their HATOL design. These bodies increase the volume by approximately 13% of the configuration total volume. The question, of course, is what do these afterbodies do to the configuration drag. The HATOL minimum drag in Fig. 22 shows several surprising findings. First, the very high experimental drag-rise Mach number (about 0.95) of this concept is unusual. It is much higher than predicted and higher than the other concepts. Also, the low level of the drag between Mach 1 and 1.4 as compared to the other concepts was an unexpected finding. Both of these results led to a number of repeat runs as a check of the data. The repeat runs gave exactly the same answers.

To further understand the minimum drag of the Northrop HATOL configuration, a component buildup test was performed (Refs. 14 and 20). Four of the eight different configuration combinations that were tested are shown in Fig. 25. This shows the relatively small drag increment (about 10 drag counts through the Mach range) that is associated with the afterbodies. This represents only about 4% of the total drag at Mach 1.1. Another

interesting finding in Fig. 25 is the large drag increment that is associated with the canards and vertical tails at subsonic speeds. By taking advantage of some of the other configuration combinations that were tested in the component buildup, a major portion of this increment was traced to an unfavorable interference of the canards on the vertical tails. This suggests an area for improvement during development of this configuration, such as the possibility of a slight repositioning of the vertical tails.

### 3.1.3.2 Wave Drag

Continuing the discussion of minimum drag, a major uncertainty is the transonic wave drag for these V/STOL fighter concepts because of the additional volume required by the propulsive lift system. This concern was identified by the contractors for all the concepts studied. The VATOL concepts should be less of a problem because they do not require as much volume for an onboard lift system as the HATOL configurations do.

To determine the penalty in wave drag for these V/STOL concepts, a comparison with existing fighter aircraft on an equal reference basis is in order. Such a comparison is shown in Fig. 26. Here the wave drag is defined as the drag coefficient increase from Mach 0.8 to 1.2. This is plotted versus the ratio of the maximum cross section area (adjusted for inlet capture area) to the square of the aircraft length. For reference, also shown on the plot is the wave drag of the Sears-Haack optimum body of revolution for a specified length and volume, and both 1.5 and 2.0 times this wave drag level. In all cases, the drag coefficient is based on the cross sectional area. Several existing fighter aircraft are represented by the open symbols and the present V/STOL model experimental results are denoted by the three solid symbols (NH = Northrop HATOL, NV = Northrop VATOL, GD = General Dynamics E205).

The wave drag of the HATOL is surprisingly low when it is compared to other fighter aircraft. The HATOL drag level is less than 1.5 times the Sears-Haack level. Again, it appears that the large afterbodies and their additional internal volume do not overly penalize the configuration in terms of wave drag.

The plot also shows the effect of proper area ruling on the E205 ejector concept. Although it has a wave drag higher than the HATOL concept, the E205 drag level is also less than 1.5 times the Sears-Haack drag level It is interesting to note that the two designs that have considerable volume dedicated to the propulsive lift system (RALS and ejectors) have wave drag levels relative to the Sears-Haack body of less than 1.5 times when compared to a factor of about 1.7 for the Northrop VATOL configuration. In fact, the VATOL configuration has a wave drag that is almost equal to that of the E205 design.

In summary, these types of V/STOL concepts can be configured to give reasonable values of wave drag when compared to existing fighter aircraft, even when the additional volume requirements of the propulsive lift system are considered. As Fig. 26 shows, the V/STOL concepts have wave drag levels that are lower than those of many of the existing fighter aircraft that have been considered. This fact dispells one of the major uncertainties that is associated with these high performance V/STOL fighter concepts, at least for these twin-engine designs. This assessment for the single-engine concepts is awaiting wind-tunnel tests of the two models.

### 3.1.3.3 High Angle-of-Attack Aerodynamics

A number of the aerodynamic uncertainties concern the high angle-of-attack flight regime for these powered lift fighter concepts, and the ability to predict these characteristics by using existing techniques. To investigate these uncertainties, the models are typically tested to approximately 90° in the Ames 12-Foot Wind Tunnel and to approximately 25° at transonic speeds in the Ames 11-Foot Wind Tunnel.

An example of this is shown in Fig. 27. The GD ejector configuration (E205) was tested to an angle of attack of 85° at Mach number 0.2 in the Ames 12-Foot Wind Tunnel. These results (Refs. 14, 16, and 22) are shown for the model with all control settings at zero. To reach these high angles of attack, two sting support arrangements are used. This is indicated by the circular and square symbols, respectively, in the figure.

A prediction method (AEROX) developed at NASA Ames (Refs. 23 and 24) to rapidly estimate nonlinear aerodynamic characteristics to high angles of attack, was used for the estimates in Fig. 27. Although it did not always predict the absolute values of the various coefficients, the trends and slopes estimated by the program are good for this unique type of configuration. This is only one example, but it appears that this approach offers potential for aerodynamic predictions to angles of attack far beyond the capability of the computational methods presently used.

The measured angle-of-attack characteristics for the GD E205 model at the higher Mach numbers are shown in Fig. 28 (Refs. 14 and 16). The control surfaces are all set to zero deflection for this component buildup. Results for the subsonic and supersonic speeds are similar. The lift and drag of the body (BN), which includes the nacelles and the baseline inboard body-nacelle strakes, and the body-plus-vertical tail (BNV) are essentially identical. Even without the outboard wing panels, these configurations generate lift coefficients of at least 0.8 because of both the large lifting area of the wide body and nacelles, and the favorable interaction between the inboard strakes and the wide body and nacelles.

Addition of the wing (BNWV) results in increased lift coefficients as expected. Adding the canard (BNWVC), which increases the total planform area by 9.3%, further increases the lift coefficients to very high values at both Mach numbers, as a result of favorable canard-wing interactions. At $M = 0.9$, this increase in lift is about 35% at $\alpha = 20°$ angle of attack; at $M = 1.2$ it is about 23% for this same angle of attack. Or considering this another way, adding the canard at a lift coefficient of 1.3 reduces the drag coefficient about 34% at $M = 0.9$ and about 21% at $M = 1.2$. As these results demonstrate, this concept offers the combination of two technologies for improved high angle-of-attack aerodynamics — close coupled canards and strakes.

### 3.1.3.4 LEX Effects

One of the uncertainties that has been identified by Northrop for the VATOL design concerns the effectiveness of the wing leading edge extension (LEX). This surface affects the longitudinal aerodynamics, the

vertical tail effectiveness, and the flow quality to the top-mounted inlet on this concept. To explore this uncertainty, three sizes of LEXs were tested on the VATOL model (Fig. 16). These were the standard size, one approximately one-half this size (alternate), and with LEX-off. The measured longitudinal characteristics are compared in Fig. 29 for Mach numbers 0.6 and 0.9. These results, taken from Ref. 19, are based on the total model planform area to give a true comparison of these lift enhancing surfaces as previously described. The results show that at angles of attack above 10° at subsonic speeds, the standard LEX improves the lift (up to 15%) and the drag as compared to the LEX-off (up to 40%). There were no lift or drag benefits from the LEX at Mach number 1.2 (Ref. 19).

As shown in Fig. 29, the larger, standard LEX gives the greater benefits in lift and drag when it is compared to the smaller LEX. As an added note, studies of LEX effects on flow quality to the top inlet of the VATOL model show the larger LEX to give the better performance at the higher angles of attack. Reference 19 further indicates that a larger canard relative to the wing size gives greater benefits when it is compared to a smaller one. Therefore, these results suggest that the larger LEXs and larger canards produce greater improvements in lift and drag, but they are limited by the control power of the elevons. Finally, Ref. 19 indicates that the benefits of the VATOL LEX and the HATOL canard are comparable in overall magnitude.

### 3.1.3.5 Aerodynamic Center

A major uncertainty that has been identified for the E205 ejector configuration is the aerodynamic center (A. C.) location and travel with Mach number. This arises because the integration of the forward ejector bays, the outboard nacelles, and the canards results in a design with a large amount of planform area that is located well forward on the aircraft. Because of this, the concern is whether the configuration has an acceptable stability at subsonic speeds, and also whether the existing prediction techniques are appropriate in the design of a unique configuration as in the E205.

Figure 30 shows the A. C. location in terms of percent mean aerodynamic chord (MAC) for the ejector model as measured in the three wind tunnels (Refs. 14, 16, and 22). All control surfaces were set at zero deflection. Results for canard-on (open symbols) and canard-off (solid symbols) configurations are shown. The experimental data show a forward A. C. location of approximately 26% at subsonic speeds for the canard-on configuration. This instability level is probably considerably higher than is desired; however, modern control-system technology is becoming sufficiently mature so that allowances can be made for such instabilities (for example, the X-29A forward-swept-wing demonstrator aircraft is about 35% unstable). However, this instability level can be affected appreciably by canard longitudinal location and strake shape. This is demonstrated in Fig. 30 by the shaded area which indicates the experimental range of A. C. location travel that is obtained for various combinations of strake shape and canard location tested on the model.

Estimates of the A. C. location, obtained by using several prediction methods, are also shown in Fig. 30. The solid and dashed lines show the estimates made by General Dynamics for the canard-on and canard-off configurations. With exception of Mach number 0.95, the estimates agree well at subsonic speeds and up to approximately Mach number 1.2. Above this speed, the A. C. location is predicted to be farther aft on both configurations than the experimental results indicate. This difference is about 5% of the MAC for the canard-on configuration.

The long- and short-dashed curve in Fig. 30 is a prediction for the canard-on configuration that was obtained by using the Ames AEROX program. The results predicted by this method are within 4% of the MAC for these measured data. The predictions shown above met with varying success for this type of configuration. Also, the calculated and measured results shown in Fig. 30 are for the low-angle-of-attack attached-flow regime. The existing prediction methods are expected to be less reliable in the nonlinear regions at higher angles of attack.

To further amplify the A. C. location of the E205 configuration as it is affected by the canard longitudinal locations and the strake shapes tested, Fig. 31 (Ref. 22) is shown. These results are for Mach 0.2 in the Ames 12-Foot Wind Tunnel, and include the small center-of-gravity shifts on the aircraft that are caused by these surface variations (generally less than 0.5% MAC). The upper portion of the figure shows that moving the canard either forward or aft of the baseline position by 25% of the wing MAC (this movement was available on the model) changes the stability by about 5.5% MAC. Changing the strake size from the large (baseline) to the strake off reduces the instability by approximately 2%. Thus on this configuration, the canard variations tested have a greater effect on stability than do the strake variations tested.

The effects of these canard and strake variations on maximum-trimmed lift coefficients $(C_{L_T})$MAX, were estimated in Ref. 22 by using canard incidence and wing-flap test data. These results are shown in the lower portion of Fig. 31. The reduced instability of the aft canard location allows a 20% increase in maximum trimmed-lift coefficient over the baseline mid position. The lift is reduced by about this same percentage by moving the canard forward. Changing from the baseline strake to strake off increases the maximum-trimmed lift by about 9%. Thus, because of their respective influences on A. C. location, the canard changes have greater effect on maximum trimmed lift than do the strake changes.

### 3.1.3.6 Buffet Onset

In-flight thrust vectoring in combat is a possibility with any of the V/STOL fighter concepts because of the inherent thrust vectoring capability that already exists in the concept. A canard is generally used on these concepts to provide trim with a positive lift and to improve the high angle-of-attack performance of the wing. This leads to an uncertainty that affects the buffet onset characteristics of these types of configurations. To investigate this uncertainty, a wing-root bending moment gauge was installed in the left wing of the GD E205 ejector model to obtain an initial indication of the angle of attack for buffet onset at transonic speeds in the Ames 11-Foot Wind Tunnel. Some measured results (Refs. 14, 16, and 17) from these tests are shown in Fig. 32 with all control surface deflections set at zero. Canard-on (baseline mid-position) and canard-off experimental data are indicated by the circular and square symbols, respectively, and appear in the upper plot of Fig. 32. At subsonic speeds, the canard gives a slight increase in the angle of attack for the onset of buffeting $(\alpha_{BO})$, but at the supersonic Mach number this trend is reversed. The predictions that are shown in Fig. 32 are obtained from Ref. 3, and are based on the correlation of results from tests of

similar configurations. The agreement at subsonic speeds is within a degree or so, but the prediction at Mach number 1.2 is approximately 4° lower than the experiment. The reversal in the effect of the canard with increasing supersonic Mach number is predicted. However, further research is needed to gain a better understanding of buffet-onset phenomena.

At the bottom of Fig. 32, measured data are shown for the three different longitudinal canard locations. At subsonic Mach numbers, the midposition (baseline) gives the higher buffet-onset angle of attack. At Mach number 1.2, there is a reversal in the effects of the canard location.

## 3.2 Airframe/Propulsion Integration

This section will briefly describe three research activities that relate to the airframe/propulsion integration characteristics of these high-performance V/STOL concepts. These include in-flight thrust vectoring, top inlets, and propulsion simulation in wind-tunnel testing.

### 3.2.1 In-Flight Thrust Vectoring

To expand the limited propulsion/airframe interaction data base on high-performance V/STOL aircraft concepts, a wind-tunnel research program was conducted at NASA Ames Research Center. The model (Fig. 33) is a one-eighth scale, twin-engine, V/STOL fighter concept developed to study various types of nozzles that are integrated into this type of configuration. The model geometry is based on the Grumman Design 623-family of configurations and is a forerunner of the RALS concept previously described in this paper and in Ref. 1. The nozzles considered in the study are a baseline circular convergent-divergent nozzle, an ADEN (Ref. 1) and an ALBEN (Asymmetric Load Balanced Exhaust Nozzle). The ALBEN, a CTOL derivative of the ADEN, features elliptical-throat and expansion-surface contours. Figure 34 shows the model with the ADEN installed on it. This nozzle on the wind-tunnel model can be tested in the cruise mode and in the thrust-deflection mode for in-flight maneuvering, but 90° thrust deflection is not available on this model.

The model includes the capability to measure forces and pressures. Extensive pressure instrumentation is installed on the wings and nacelles to isolate the propulsion-induced effects. The model is supported by twin vertical tails (Fig. 33), which also provide passage for high-pressure air for jet-effects testing. Tests were conducted in the Ames 11-Foot Transonic Wind Tunnel for Mach numbers from 0.4 to 1.4. Some of the results (Refs. 25-28) are summarized here.

The unvectored-ADEN and the ALBEN nozzles are competitive on a thrust-removed drag polar basis, an example of which is shown in Fig. 35 (see Ref. 26). Both of these nozzles show large performance gains, at all flight conditions, relative to the circular nozzle. For example, a typical cruise drag reduction of 50 counts (0.0050) at Mach 0.9 is shown in Fig. 35. However, some of this drag increment is due to the difficulty of integrating a circular nozzle exit with a straight wing trailing edge. The influence of thrust-vectoring for this ADEN (installed at the trailing-edge of the wing in the root area) travels very far upstream and spanwise nearly to the wing tip. This results in significant jet-induced lift as indicated by the example in Fig. 36 (Ref. 26) of the ADEN cruise lift build-up. This shows the jet-off aerodynamic lift, the jet-induced lift, and the jet lift itself.

When vectoring the ADEN, an optimum polar locus is formed by an envelope of points that cover a range of deflection angles. This means that deflection angle should be scheduled with angle of attack to achieve optimum performance. In general, larger thrust-vectoring advantages are measured as the subsonic Mach number is reduced. No vectoring benefits were found at supersonic speeds in this research program.

At a key Mach 0.9 cruise nozzle (nonafterburning) condition (CL = 0.3), a 40-count drag reduction is realized as the ADEN is vectored from 0° to 10° in Fig. 37 (Ref. 26). When this thrust vectoring payoff is combined with the previously described 50-count reduction of the cruise ADEN versus the circular nozzle, a 90-count reduction is achieved for the vectored ADEN over the baseline circular nozzle installation. This 90-count reduction represents 25% of the zero-lift drag for this V/STOL concept. Finally, at Mach 0.9 maneuver conditions, only moderate (about 10°) deflection angles of the ADEN combat (maximum afterburning) nozzle are expected to provide advantage, because larger deflections cause nozzle thrust losses and induced-drag penalties.

### 3.2.2 Top Inlet

In the previously described studies of V/STOL fighter/attack aircraft concepts, top-mounted air induction systems have been identified as a very promising and desirable design feature. This inlet location offers a number of significant advantages when compared with conventional locations, including (1) decreased ingestion of debris and hot gases during takeoff and landing, (2) reduction in radar cross section, and (3) improved weapons integration. However, there are a number of concerns with top-mounted inlets, including increased upper-surface local Mach number at the higher angles of attack because of flow expansion, particularly at the higher Mach numbers. Other concerns include possible ingestion of (1) distorted flows at high angle of attack, (2) vortices from a canard or wing leading-edge extension (strake), and (3) low-energy boundary layers. A major concern is the lack of aerodynamic data on these types of inlets at higher speeds on which to base aircraft design studies. Because of this and the desirable features of top-mounted inlets, a program, jointly sponsored by Ames and the David Taylor Naval Ship Research and Development Center (NSRDC), was initiated to develop an aerodynamic data base on this promising technology.

To explore top inlet performance, the previously described Northrop VATOL model (Fig. 17) was provided with additional components and instrumentation (Fig. 38). This included remotely controlled mass flow control plug assemblies, inlet flow-field instrumentation at the inlet face to measure flow pressures and direction, and steady state and dynamic pressure instrumentation located at the simulated engine compressor face.

The LEX on the wing is the key to the top inlet performance on the present VATOL concept. These surfaces produce a strong, counter-rotating vortex pair which effectively inhibits upper-fuselage flow separation by entraining high-energy free-stream air into the upper-fuselage region and by sweeping low-energy boundary layer air outward. Thus the LEX size is an important parameter to investigate, as well as other geometric features that affect the upper inlet flow field. The following airframe variations were tested in the research

program: (1) LEX size and the absence of LEX, (2) wing leading-edge flap deflection, (3) canopy-on and canopy-off, and (4) canard integration and deflection. Tests were conducted in the Ames 11-Foot and 9- by 7-Foot Wind Tunnels over a Mach number range of 0.6 to 2.0. Angle of attack was varied to approximately 28° subsonically and to approximately 18° at the highest supersonic speeds. Angle of sideslip was varied up to 8° to 10°.

This research program generated extensive data on top-inlet flow field and engine-inlet performance characteristics at subsonic, transonic, and supersonic speeds. The significant findings from this wind-tunnel test program are presented in Refs. 29 through 34.

One example result is the summary of the measured distortion effects with angle of attack and angle of sideslip as shown in Fig. 39 (see Ref. 29). Distortion is defined here as the maximum minus the minimum pressure recovery at the compressor face divided by the average pressure recovery. In Fig. 39, distortion-limited operating envelopes are shown for Mach numbers 0.9 and 1.2 as a function of angle of attack and angle of sideslip. Both windward and leeward results are shown. The estimated airplane operating envelope and the wind-tunnel test envelope are outlined for both Mach numbers. The top figures are for a distortion level of less than 0.2 (cross hatching) and the bottom curves are for less than 0.15. In both cases, the white areas represent distortion values above these two levels. The higher distortion level ($\leq 0.2$) is considered to be acceptable to the particular turbojet engine proposed for this design. As the results show, the top inlet provides good performance over the envelope tested particularly, at the lower Mach number. Some of the problem areas (indicated in Fig. 39), particularly at Mach number 1.2, were shown during the test to be associated with the wake that was generated by the LEX/fuselage intersection. Configuration tailoring in this region could substantially reduce or eliminate these problems.

To demonstrate the potential of this top inlet system, a comparison of pressure recovery with that of other fighter aircraft using more conventional inlet installations is shown in Fig. 40 (see Ref. 31). The comparison aircraft include the YF-16 with a fuselage-shielded inlet system, the YF-17 prototype with a wing-shielded inlet, and an advanced Northrop fighter configuration with side-mounted, two-dimensional external compression inlets with fixed, vertical ramps. The comparisons are shown at Mach numbers 0.9, 1.6, and 2.0. Note that the results reflect differences in inlet design and mission requirements and do not allow a precise comparison of the relative merits of the various systems. Rather, the comparisons serve only as an indication of the potential for the present VATOL top-inlet system.

A number of comments concerning the results in Fig. 40 are in order. In the cruise angle-of-attack range ($\alpha = 0$ to $\sim 3°$), the top inlet system provides recoveries that are comparable to those of the other aircraft at all three Mach numbers. At the transonic speed (M = 0.9), the top inlet is competitive to the maximum $\alpha$ tested, 25°. At supersonic speeds, the top inlet performance deteriorates with angle of attack primarily because of the flow field expansion which increases local inlet Mach number and causes higher inlet shock losses. In contrast, the recoveries of the shielded inlet systems improve with angle of attack because of the flow-field precompression that is provided by the forebody and/or wings.

Because of load factor constraints, the angles of attack at supersonic speeds for fighter aircraft are typically limited to 15° and 10° at Mach 1.6 and 2.0, respectively. Figure 40 shows that at these conditions, the present top inlet system gives "adjusted" recoveries that are not significantly lower than those of the other systems. The "adjusted" curves reflect the performance that is obtainable if the previously mentioned low pressure wake regions that are generated by the LEX/fuselage juncture could be eliminated by minor configuration tailoring. Note that the present top inlet system has not undergone the many hours of developmental testing that each of the other systems in Fig. 40 has. The top inlet performance could be improved with similar development efforts.

In summary, considering both the distortion level envelopes and the recovery comparisons, the top inlet is considered a viable option for these V/STOL fighter aircraft. Additional research work is needed, but considering the stated advantages of top inlets for these types of aircraft, this research effort is expected to continue.

3.2.3 Propulsion Simulation

The V/STOL concepts previously described are characterized by closely coupled inlets, canards, wing, and nozzles. Because of the interactions of the aerodynamic and propulsive flows on these "close coupled" configurations, the conventional methods of wind-tunnel testing may not give the proper results. The conventional methods consist of testing two models, a flow-through and a jet-effects model, and then combining these results into overall aerodynamic performance. However, this technique will not measure the above mentioned interactions. Therefore, a new method of wind-tunnel testing fighter aircraft that uses compact multimission aircraft propulsion simulators (CMAPS) is being pursued jointly at Ames Research Center and at the U.S. Air Force Wright Aeronautical Laboratories. This development will allow simultaneous simulation of both inlet and nozzle flows on a wind-tunnel model.

The details of this new test technique have been described in another lecture in this series (Ref. 35). Thus, only a few comments will be given here. Figure 41 shows the components of the propulsion simulator program and Refs. 36 through 41 give additional information. The simulator (upper right) is powered by high pressure air that drives a single-stage turbine which in turn drives a four-stage axial flow compressor. The simulator is approximately four inches in diameter and approximately ten inches long. Other elements of the program in Fig. 41 are the simulator control system and the calibration laboratory which is being constructed at Ames. This facility will allow complete and accurate calibration of a model containing two simulators. Also shown at upper left is the first wind-tunnel model to be tested with two of these simulators installed in it.

This model has been tested in the flow-through and jet-effects modes, and this past year it was tested with propulsion simulators installed on it. The model, which is shown in the 11-Foot Transonic Wind Tunnel in Fig. 42, simulates a wing-canard, twin-engine, high-performance STOL fighter configuration with deflectable nonaxisymmetric exhaust nozzles. Both force and pressure data were obtained in the test. Two examples of the results that are shown here are taken from Ref. 41.

One purpose of the test was to explore the ability of the CMAPS to simulate full-scale engine conditions in terms of inlet mass flow ratio (MFR) and nozzle pressure ratio (NPR). During this first test, a conservative approach was taken, and the angle-of-attack/MFR combinations were selected so that the maximum distortion would not exceed 25% based on the results of the flow-through test. The intent was to reduce CMAPS blade stresses and to minimize the possibility of compressor stall. Also, a 1,000-psi limit was placed on the turbine drive air for this test.

The demonstrated MFR range of the CMAPS with the model baseline inlet is shown in Fig. 43. At Mach numbers less than 0.9, the CMAPS upper airflow set points were limited to less than the maximum possible by the distortion limit of 25%. Alternate inlets with different lower-lip configurations were not tested, but if they had been, they would have permitted operation at maximum airflow and higher angles of attack at Mach numbers below 0.9. The lower airflow set points were based on a selected turbofan cycle and were greater than the windmill airflow and, thus, fall within the CMAPS/MFR envelope.

The demonstrated NPR envelope of the CMAPS is shown in Fig. 44. This figure shows the maximum and minimum values of NPR that were set for each Mach number. The minimum NPR boundary is determined by the windmilling operation of the simulator. The maximum NPR boundary is determined by the 1,000-psi limit on turbine drive pressure. The flow-through model NPR operating line is shown for reference. It is seen that the CMAPS can easily simulate flow-through NPR values. The upper line, labeled Pt2/Pto = 1.0, indicates the approximate maximum NPR that could be achieved with this exhaust nozzle throat area with 100% inlet recovery, low distortion, and no turbine drive pressure restriction. The NPR range of the CMAPS is limited when compared with a jet-effects simulator. The maximum NPR for a jet effects simulator is limited only by the design pressure of the chamber inside the model. The minimum is NPR = 1.0, or jet off, which is lower than the CMAPS windmill NPR. However, both the NPR and airflow range of the CMAPS are sufficient to investigate the operating range of the existing engines and a majority of advanced cycle engines.

## 4. LARGE-SCALE RESEARCH

This section of the paper describes a number of research programs in which large-scale wind-tunnel models are used to address the aerodynamic performance and the propulsion/airframe integration aspects of V/STOL fighter aircraft. This research takes place at low speed and under static test conditions. Tests are typically conducted in the Ames 40- by 80-Foot Wind Tunnel and at the Ames Outdoor Aerodynamic Research Facility (OARF). The 80- by 120-Foot Wind Tunnel will become a part of this test complex in the near future.

As an example of the type of tests that are conducted in these facilities, a full-scale model of the AV-8B with a Pegasus engine is shown mounted in the Ames 40- by 80-Foot Wind Tunnel in Fig. 45. Tests were conducted at thrust levels of up to 16,500 lb at speeds approaching 180 knots. The nozzle deflection was limited to 65° because of model size relative to that of the test section. It is expected that operation of such a model in the Ames 80- by 120-Foot Test Section will not be as restrictive in thrust deflection. Figure 46 shows the same model at the OARF. Forces are measured by load cells that are located at the support attachment points.

The large-scale V/STOL fighter research activities that are summarized in this section include a twin-engine fighter model and tests, high angle-of-attack studies, and thrust-augmenting ejector research.

### 4.1 Twin-Engine Model

A large-scale wind-tunnel model of a twin-engine V/STOL fighter is described in this section. This model has been tested in the Ames 40- by 80-Foot Wind Tunnel and an example of the results is given.

### 4.1.1 Model Description

Many of the uncertainties that affect aerodynamic performance of V/STOL fighter aircraft exist at the hover- and low-speed transition conditions. Because of this, NASA Ames is conducting a research program that is centered around a large-scale wind-tunnel model of a twin-engine supersonic V/STOL fighter. The configuration selected for this research is the General Dynamics E205 configuration. This concept, described early in this paper, was derived in the Phase I studies of Ref. 3, and is further described in Ref. 1. The large-scale model currently does not have the ejector propulsive lift system installed, but rather is configured in a STOL fighter configuration. Figure 47 shows the model that is installed in the Ames 40- by 80-Foot Wind Tunnel and Fig. 48 gives the model geometry. The 7.28-m (23.9-ft) span model is equipped with close-coupled canards and an aft fuselage control (beaver tail) for pitch control. The canard, with leading- and trailing-edge flaps, can be mounted in three longitudinal positions to investigate canard/wing interference. The beaver tail is intended primarily as a takeoff and landing pitch trim device. Roll and secondary pitch control are provided by the outboard wing trailing-edge flaps (ailerons) which are normally set at a geometric angle that is close to those of the inboard wing flap (primary nozzle flap).

The model is powered by two General Electric J-97 turbojet engines, each producing 9,340-N (2,200-lb) thrust at a pressure ratio of 2.0. The engines are mounted in nacelles at 33% semispan. This provides a large strake area (inboard of the nacelles) for possible future integration of an ejector system to give the model VTOL capability. The nacelles are somewhat oversized in comparison to the E205 design to accommodate the J-97 engine. The model combines two propulsive-lift technologies, upper-surface blowing (USB) and spanwise blowing (SWB) to augment the lift over a wide angle-of-attack range. As shown in Fig. 49, the J-97 exhausts into a transition duct where 16% of the flow can be diverted to the SWB system to delay wing stall by augmenting the wing leading-edge vortex. The remaining 84% of the engine flow exhausts into a two-dimensional, half-wedge, convergent-divergent nozzle. This nozzle preturns the flow down 25°, and exhausts over the nozzle flap upper surface, providing exhaust vectoring capability from -10° to 40°. This propulsion system is an adaptation of the vectored engine-over wing (VEO-wing) concept developed by General Dynamics (Refs. 42 and 43).

The SWB exhausts at a 34° sweep-back angle, as measured in static tests, from a rectangular nozzle that is flush with the nacelle outer wall approximately 1.5 nozzle heights above the wing surface. When the model is

tested without SWB, this nozzle is covered and the two-dimensional USB nozzle area is increased to maintain the same overall exhaust area. The thrust characteristics and flow turning angles for each nacelle were measured at the Ames Static Test Facility. The results of these static tests and a complete propulsion system description are reported in Ref. 44.

### 4.1.2 Tests and Results

The model has undergone three investigations in the Ames 40- by 80-Foot Wind Tunnel and one investigation at the Ames Static Test Facility. During these studies, the characteristics of the flow surrounding the airframe, as well as overall aerodynamic force and moment characteristics, were investigated. The model was equipped to measure the surface pressure on the canard, wing, strake, and flaps as well as total pressure distributions in the propulsion system exhaust. The location of the surface taps can be seen as the dark lines on the port side of the model in Fig. 47. The surface of the wing was also instrumented to measure surface air temperature to study the environment to which the wing will be exposed by SWB.

A summary of the results of tests of this model are given in Refs. 45 through 47. Basic longitudinal characteristics are given in Ref. 45 for nozzle thrust vector angles ($\delta_T$) of 40°, 18°, and -1°. An example is given in Fig. 50 for $\delta_T = 18°$, with SWB on and the canard in the aft position. Power strongly affects lift characteristics over the entire alpha range. The combination of USB and SWB generates maximum lift coefficients well in excess of four at high-thrust coefficients with gentle stall characteristics. The maximum lift generated is even higher for $\delta_T = 40°$ (Ref. 45). At $\alpha = 15°$, USB induces a 10% to 15% increase in lift. Spanwise blowing provides an additional 10% to 13% improvement in lift. Other significant findings are presented in Refs. 45 through 47.

### 4.2 High Alpha Research

A research program to study the high angle-of-attack aerodynamic performance of V/STOL fighter aircraft at low speed is being conducted at Ames Research Center using large-scale models. Of primary interest in this program is the use of vortex lift to enhance the high-lift aerodynamic characteristics and the ability to predict the resulting complex and interacting flows. This is of concern for fighter aircraft during maneuvering flight and is of additional concern for V/STOL fighter aircraft during transition flight. A brief description of one model and test will be given here as an example of the type of activity in this research program. The material presented is taken from Refs. 48 through 51.

### 4.2.1 Model Description

In this research program, a well-instrumented, large-scale powered model of a close-coupled canard-delta-wing V/STOL fighter configuration was tested in the Ames 40- by 80-Foot Wind Tunnel. It is a 0.4-scale model of a design that was developed by Vought in the studies of Ref. 7. The concept was briefly described earlier and was further described in the Ref. 1 paper. The model that is shown is installed in the 40- by 80-Foot Wind Tunnel (Fig. 51), and the model geometry is given in Fig. 52.

For these high angle-of-attack studies, a sting-type of support system is used (Fig. 51). The model is sting-mounted with the wing chordplane in a vertical position so that rotation of the wind-tunnel turntable allows testing through 90° angle of attack. Figure 53 indicates how both pitch and yaw are obtained. The 12-in. diam tip-driven fans provide inlet airflow and low-velocity exhausts. Adjustable control surfaces included canard incidence, canard trailing-edge flaps, and wing leading- and trailing-edge flaps. Force and moment data were measured by an internal six-component strain gauge balance. Approximately 500 pressures were measured to document the model surface and duct pressure distributions, and the power conditions. The model was tested to about 110° angle of attack, at several angles of sideslip, and at several power levels. Canard and flap variations were made, and canard-on and canard-off configurations were investigated. The results from the test are given in Refs. 48 through 51.

### 4.2.2 Tests and Results

An example of the high angle-of-attack longitudinal aerodynamic characteristics that were measured during the test is shown in Fig. 54 (Ref. 51). The power-removed results are for canard-on and canard-off configurations. The lift curves are nearly identical up to an angle of attack of 10°, beyond which the canard-on model achieves greater lift. Both configurations reach maximum lift at approximately 33° angle of attack. Although the canard adds only 15% more area over the wing reference area, a 34% increase in maximum lift is achieved.

An attempt was made to predict the above longitudinal aerodynamics in the high angle-of-attack regime, which is characterized by a complete absence of attached flow or attached vortex flow on the top-side of the lifting surfaces. To make these predictions, a flat-plate analogy was used which is described in Ref. 51. Figure 55 (see Ref. 51) gives the results of the predictions. With exception of the pitching moment, the estimates of the model longitudinal characteristics in the fully stalled angle-of-attack range were good.

### 4.3 Ejector Research

For several years, Ames Research Center has conducted research on thrust augmenting ejectors for application to powered-lift aircraft. The objective has been to evaluate the fluid dynamics of the ejector itself and to integrate it with the complete propulsive lift system. This has involved fundamental ejector development, small- and large-scale tests, and the application and development of prediction techniques. An important guideline in all of these programs is the ability to package the ejector system within the lines of the aircraft configuration. The research activities have included ejectors that are applicable to both the STOL and the V/STOL aircraft. The present discussion will be limited to a brief summary of several efforts that are related to V/STOL fighter aircraft. Reference 52 gives an excellent review of these research activities.

There are three types of ejectors that are considered for fighter aircraft that have a vertical flight capability (see Fig. 56). All three types have been used in several of the V/STOL fighter concepts described

in this paper and in Ref. 1. The research activities that are related to the "fuselage ejector" and the "short diffuser ejector" are summarized below. The "spanwise ejector" is the type of ejector that was used in the XFV-12A Thrust Augmentor Wing aircraft that was built and tested by Rockwell International.

### 4.3.1 Fuselage Ejector

The fuselage ejector was initially proposed by de Havilland Aircraft of Canada Ltd., and research has continued to be supported jointly by NASA and Canada. These efforts are summarized in Refs. 52-55. This type of ejector is considered for designs where part of the fuselage is used for one side of the diffuser with the other side provided by a retractable lower door as indicated by Fig. 56. An advantage of this ejector over the short-diffuser type and the spanwise types is mechanical simplicity, and possibly, flow stability because of the long diffuser.

The development of the fuselage ejector was first accomplished by component development and testing using laboratory models. Verification of the results from these component and small-scale tests is provided by the large-scale model shown in Fig. 57. This generic model is installed in the Ames 40- by 80-Foot Wind Tunnel and is powered by a J97 engine. The two ejector bays with the numerous spanwise ejector lobes are evident in the figure. Several wind-tunnel tests of this model have provided a valuable data base for treating induced effects and transition performance. These tests proved that there is a need to deflect the ejector thrust from the vertical position so that sufficient thrust could be provided for transition. An effective way to accomplish this is to swivel the primary nozzle lobes. Some initial testing has been done to evaluate this method.

The J97 powered model (Fig. 57) currently includes an improved method of swiveling the primary nozzle lobes for additional ejector thrust deflection (from vertical) and includes the redesign of the primary nozzles to improve mixing. Extensions to the research effort include continued development of the ejector itself and the capability to add rear thrust which can be varied in deflection, location, and jet shape. This simulated vectored core thrust was recently tested in combination with the ejectors in hovering tests at the OARF. The core thrust was vertically deflected near the rear of the model. Tests were conducted at heights of 12 ft and at the 2-ft wheel height above the ground. Future additions to the model include different wing planforms and airfoil shapes, as well as the possible addition of a canard. Alternate trailing-edge flaps will include both unblown and blown concepts.

As previously mentioned, a program is underway to incorporate the "fuselage ejector" concept together with a deflected thrust nozzle into the General Dynamics-E7 configuration. Among the several test activities in this program is an effort to further evaluate and develop the ejector system. To accomplish this, a one-third-scale, half-span powered model of the E7 configuration has been tested in the NASA Lewis 9- by 15-Foot Wind Tunnel. The model installed in the tunnel is shown in Fig. 58. The test was run with the tunnel sidewalls removed in an open test section configuration. The powered ejector lobes are evident in the figure. For this test, the inlet was faired over and the aft two-dimensional deflecting nozzle was not used. The Mach number was varied from zero (static tests) to 0.185, which is approximately the end of the transition speed for the concept. Angle of attack was varied from 0° to about 20° and a few sideslip runs were made. The outcome of the test was a verification of the ejector performance.

Another effort that relates to the E7 concept is the design and fabrication of a large-scale, engine-powered model for tests in the Ames 40- by 80-Foot Wind Tunnel in approximately three years. The objective of this program is to demonstrate the engine/airframe integration, including the incorporation of the "fuselage type" ejector system and the deflecting two-dimensional nozzle. This is a joint effort among many groups including NASA, the Canadian Government, General Dynamics, de Havilland, and Pratt and Whitney. Finally, a joint NASA Lewis/General Dynamics program to validate the propulsion system for an E7 technology demonstration aircraft (ducting, air collector, full-scale ejector, etc.) was begun in the Fall of 1983; the first tests are scheduled for the Spring of 1985.

### 4.3.2 Short Diffuser Ejector

The short diffuser ejector (Fig. 56) was developed by Flight Dynamics Research Corporation, and recent development work has been jointly sponsored by NASA and the Navy (Refs. 56 and 57). This chordwise ejector system is the concept that is used by General Dynamics (Ref. 3) in their twin-engine V/STOL fighter design (E205) that is described earlier in this paper and in Ref. 1. The ejector uses two sets of nozzles, a primary jet and a diffuser boundary layer control (BLC) nozzle as shown by Fig. 59. The purpose of the latter nozzle is to entrain the flow to the diffuser walls in the mixing section. In the current design, there is a flow split of 60% to the upper nozzles and 40% to the lower nozzles. An important part of the development of this ejector system has been to lower the upper nozzle envelope to minimize the "doors closed" length of the ejector while still maintaining the high augmentation ratio. The purpose of this is to package the ejector system within the inner wing/strake area of the E205 configuration during the up-and-away flight mode.

Up until recently, the majority of work on this ejector concept has included tests of small-scale models at low NPR. These tests indicated that an augmentation ratio of 2.1 is possible. Higher NPRs will reduce this value to something below 2.0. To investigate the performance of this ejector system as it is packaged in the E205 configuration, a 0.2-scale model will be tested in the Ames 7- by 10-Foot Wind Tunnel. This model is a semispan simulation of the E205 as shown in Fig. 60 and it is currently under construction at Ames; plans are to test it statically (approximately mid-1984) before it is tested in the 7- by 10-Foot Wind Tunnel.

### 4.3.3 Ejector Performance

Ames Research Center has studied the ejector for powered-lift applications for a number of years. A commonly used summary of ejector performance is presented in Fig. 61. Augmentation ratio, $\phi_I$ (ratio of ejector thrust to isentropic thrust of the primary nozzle), is shown versus a gross indication of the packaging capability of the ejector, $L/\bar{t}$. This is the ratio of ejector length to a given average nozzle size. Thus the objective in the research programs has been to move the performance and geometry of thrusting ejectors in hovering aircraft up, and to the left of, the plot in Fig. 61. A description of the various ejector concepts in the figure is given in Ref. 52. One important point that arises from this broad ejector research program

is that aircraft development should proceed only after a theoretical and experimental data base is accumulated on the ejector itself. This data base should include not only small-scale ejector and complete configuration wind-tunnel testing, but also full- or large-scale testing using "boiler plate" models of both aircraft components and complete configurations.

## 5. CONCLUDING REMARKS

A research effort in the United States to develop the technology for a V/STOL or STOVL fighter aircraft in the post-1995 time period has been summarized in this paper. Emphasis has been on aerodynamic performance and airframe/propulsion integration research programs that have been conducted at the Ames Research Center, the NASA lead center for powered lift aircraft. The activities summarized are, in the most part, joint NASA, Navy, and Industry programs, which represent the major V/STOL fighter aircraft efforts in the U.S. The research activities include both small- and large-scale wind-tunnel programs.

An effort has been made to focus on aerodynamic uncertainties that are associated with configuration features resulting from the V/STOL requirement. Example uncertainties are those related to minimum drag, wave drag, high angle-of-attack characteristics, and power-induced effects. An observation from this extensive research effort is that a majority of the aerodynamic and airframe/propulsion uncertainties are configuration-dependent and must be explored by use of wind-tunnel models that are representative of actual configurations as contrasted to "generic" models. This has been the direction of both the small- and large-scale research efforts at Ames.

## 6. REFERENCES

1. Nelms, W. P., and Anderson, S. B., "V/STOL Concepts in the United States — Past, Present, and Future." AGARD-FDP-VKI Lecture Series No. 7 on V/STOL Aerodynamics, von Karman Institute, Belgium, May 14-18, 1984.

2. Nelms, W. P., "Studies of Aerodynamic Technology for VSTOL Fighter/Attack Aircraft." AIAA Paper 78-1511, August 1978.

3. Lummus, J. R., "Study of Aerodynamic Technology for VSTOL Fighter/Attack Aircraft." NASA CR-152128, 1978.

4. Burhans, W. R., Crafa, V. J., Dannenhoffer, N. F., Dellamura, F. A., and Krepski, R. E., "Study of Aerodynamic Technology for VSTOL Fighter/Attack Aircraft." NASA CR-152129, 1978.

5. Brown, S. H., "Study of Aerodynamic Technology for VSTOL Fighter/Attack Aircraft — Horizontal Attitude Concept." NASA CR-152130, 1978.

6. Gerhardt, H. A., and Chen, W. S., "Study of Aerodynamic Technology for VSTOL Fighter/Attack Aircraft — Vertical Attitude Concept." NASA CR-152131, 1978.

7. Driggers, H. H., "Study of Aerodynamic Technology for VSTOL Fighter/Attack Aircraft." NASA CR-152132, 1978.

8. Nelms, W. P., and Durston, D. A., "Concept Definition and Aerodynamic Technology Studies for Single Engine VSTOL Fighter/Attack Aircraft." AIAA Paper 81-2647, December 1981.

9. Foley, W. H., Sheridan, A. E., and Smith, C. W., "Study of Aerodynamic Technology for Single-Cruise-Engine VSTOL Fighter/Attack Aircraft." NASA CR-166268, 1982.

10. Foley, W. H., "An Integrated Aerodynamic/Propulsive Design for a STOVL Fighter/Attack Aircraft." ICAS-82-1.6.2, 1982.

11. Mark, L., "Study of Aerodynamic Technology for Single-Cruise-Engine VSTOL Fighter/Attack Aircraft." NASA CR-166270, 1982.

12. Hess, J. R., and Bear, R. L., "Study of Aerodynamic Technology for Single-Cruise-Engine VSTOL Fighter/Attack Aircraft." NASA CR-166269, 1982.

13. Driggers, H. H., "Study of Aerodynamic Technology for Single-Cruise-Engine VSTOL Fighter/Attack Aircraft." NASA CR-166271, 1982.

14. Nelms, W. P., and Durston, D. A., "Preliminary Aerodynamic Characteristics of Several Advanced VSTOL Fighter/Attack Aircraft Concepts." SAE Paper No. 801178, October 1980.

15. Nelms, W. P., Durston, D. A., and Lummus, J. R., "Experimental Aerodynamic Characteristics of two VSTOL Fighter/Attack Aircraft Configurations at Mach Numbers from 0.4 to 1.4." NASA TM-81234, December 1980.

16. Lummus, J. R., Joyce, G. T., and O'Malley, C. D., "Analysis of Wind Tunnel Tests Results for a 9.39% Scale Model of a VSTOL Fighter/Attack Aircraft." NASA CR-152391, Vols. 1-4, January 1981.

17. Lummus, J. R., "Aerodynamic Characteristics of a VSTOL Fighter Configuration." AIAA Paper 81-1292, 1981.

18. Nelms, W. P., Durston, D. A., and Lummus, J. R., "Experimental Aerodynamic Characteristics of Two VSTOL Fighter/Attack Aircraft Configurations at Mach Numbers from 1.6 to 2.0." NASA TM-81286, May 1981.

19. Durston, D. A., and Smith, S. C., "Lift Enhancing Surfaces on Several Advanced VSTOL Fighter/Attack Aircraft Concepts." AIAA Paper 81-1675, August 1981.

14

20. Moore, W. A., "Wind Tunnel Data Analysis of the Northrop Horizontal Attitude VSTOL Fighter Configuration for Mach Numbers from 0.4 to 1.4." NASA CR-166277, 1982.

21. Moore, W. A., "Wind Tunnel Data Analysis of the Northrop Vertical Attitude VSTOL Fighter Configuration for Mach Numbers from 0.4 to 1.4." NASA CR-166278, 1982.

22. Durston, D. A., and Schreiner, J. A., "High Angle of Attack Aerodynamics of a Strake-Canard-Wing V/STOL Fighter Configuration." AIAA Paper 83-2510, October 1983.

23. Axelson, J. A., "Estimation of Transonic Aircraft Aerodynamics to High Angles of Attack." J. Aircraft, Vol. 14, June 1977, pp. 553-559.

24. Axelson, J. A., "AEROX — Computer Program for Transonic Aircraft Aerodynamics to High Angles of Attack, Vols. I, II, III." NASA TM X-73,208, 1977.

25. Schnell, W. C., and Ordonez, G. W., "Axisymmetric and Non-Axisymmetric Exhaust Jet Induced-Effects on a VSTOL Vehicle Design, Part I — Data Presentation." NASA CR-166146, 1981.

26. Schnell, W. C., "Axisymmetric and Non-Axisymmetric Exhaust Jet Induced-Effects on a VSTOL Vehicle Design, Part II, Analysis of Results." NASA CR-166365, 1982.

27. Schnell, W. C., and Ordonez, G. W., "Axisymmetric and Non-Axisymmetric Exhaust Jet Induced Effects on a VSTOL Vehicle Design, Part III, Experimental Technique." NASA CR-166147, 1981.

28. Smeltzer, D. B., and Levin, A. D., "Test Results from a Jet-Effects VSTOL Fighter Model with Vectoring Non-Axisymmetric Nozzles." NASA TM-81210, June 1980.

29. Smeltzer, D. B., Nelms, W. P., and Williams, T. L., "Airframe Effects on a Top-Mounted Inlet System for VSTOL Fighter Aircraft." AIAA Paper 81-2631, December 1981.

30. Smeltzer, D. B., Nelms, W. P., and Williams, T. L., "Airframe Effects on a Top-Mounted Fighter Inlet System." AIAA Paper 81-2631R, J. of Aircraft, Vol. 19, No. 12, December 1982.

31. Williams, T. L., Hunt, B. L., Smeltzer, D. B., and Nelms, W. P., "Top-Mounted Inlet System Feasibility for Transonic-Supersonic Fighter Aircraft." AGARD Fluid Dynamics Panel Symposium, May 1981.

32. Williams, T. L., Nelms, W. P., and Smeltzer, D. B., "Top-Mounted Inlet System Feasibility for Transonic-Supersonic Fighter Aircraft." NASA TM-81292, April 1981.

33. Durston, D. A., and Smeltzer, D. B., "Inlet and Airframe Compatibility for a V/STOL Fighter/Attack Aircraft with Top-Mounted Inlets." NASA TM-84252, June 1982.

34. Durston, D. A., and Smeltzer, D. B., "Inlet and Airframe Compatibility for a V/STOL Fighter/Attack Aircraft with Top-Mounted Inlets." ICAS Paper 82-4.2.2, Proceedings from 13th Congress of the International Council of the Aeronautical Sciences and AIAA Aircraft Systems and Technology Conference, Vol. 2, August 1982.

35. Koenig, D. G., "V/STOL Wind Tunnel Testing." AGARD-FDP-VKI Lecture Series No. 7 on V/STOL Aerodynamics, von Karman Institute, Belgium, May 14-18, 1984.

36. Eigemann, M. F., and Bailey, R. O., "Development of the Propulsion Simulator — A Test Tool Applicable to VSTOL Configurations." SAE Paper No. 770984, November 1977.

37. Bailey, R. O., Harper, M., and Janetta, T., "Evaluation of Turbo-Propulsion Simulators as a Testing Technique for Fighter Aircraft." AIAA Paper 79-1149, June 1979.

38. Bailey, R. O., Mraz, M., and Hiley, P., "The Design of a Wind Tunnel VSTOL Fighter Model Incorporating a Turbine Powered Engine Simulator." AIAA Paper 81-2635, December 1981.

39. Harper, M., "The Propulsion Simulator Calibration Laboratory at Ames Research Center." AIAA Paper 82-0574, March 1982.

40. Smith, S. C., "Determining Compressor Inlet Airflow in the Compact Multimission Aircraft Propulsion Simulators in Wind Tunnel Applications." AIAA Paper 83-1231, June 1983.

41. Bailey, R. O., Smith, S. C., and Gustie, J. B., "Propulsion Simulation Test Technique for V/STOL Configurations." SAE Paper 83-1427, October 1983.

42. Whitten, P. D., "An Experimental Investigation of Vectored-Engine-Over-Wing Powered Lift Concept." AFFDL-TR-7692, 1978.

43. Bradley, R. G., Jeffries, R. R., and Capone, F. J., "A Vectored-Engine-Over-Wing Propulsive Lift Concept." AIAA Paper 76-917, September 1976.

44. Harris, M. J., and Falarski, M. D., "Static Calibration of a Two-Dimensional Wedge Nozzle with Thrust Vectoring and Spanwise Blowing." NASA TM-81161, 1980.

45. Falarski, M. D., Whitten, P. D., and Harris, M. J., "Aerodynamic Characteristics of a Large-Scale Model of a Highly Maneuverable Supersonic V/STOL Fighter: STOL Configuration." AIAA 80-0234, January 1980.

46. Howell, G. A., Crosthwait, E. L., and White, M. C., "Evaluation of Pressure and Thermal Data from a Wind Tunnel Test of a Large-Scale, Powered, STOL Fighter Model." NASA CR-166170, June 1981.

47. Falarski, M., Dudley, M., and Howell, G., "Analysis of Data From a Wind Tunnel Investigation of a Large-Scale Model of a Highly Maneuverable Supersonic V/STOL Fighter: STOL Configuration." AIAA Paper 81-2620, December 1981.

48. Stoll, F., and Minter, E., "Large-Scale Wind Tunnel Tests of a Sting-Supported V/STOL Fighter Model at High Angles of Attack." AIAA Paper 81-2621, 1981.

49. Minter, E. A., and Yates, R. W., "Wind Tunnel Test of a 0.4-Scale Fighter Model at High Angles of Attack — Analysis of Pressure Data." NASA CR-166198, 1981.

50. Stoll, F., and Koenig, D. G., "Low Speed Wind Tunnel Measurements of a Canard Controlled Fighter Model Through High Angles of Attack." NASA TM-84403, 1983.

51. Stoll, F., and Koenig, D. G., "Large-Scale Wind-Tunnel Investigation of a Close-Coupled Canard-Delta-Wing Fighter Model Through High Angles of Attack." AIAA Paper 83-2554, October 1983.

52. Koenig, D., Stoll, F., and Aoyagi, K., "Application of Thrusting Ejectors to Tactical Aircraft Having Vertical Lift and Short-Field Capability." AIAA Paper 81-2629, December 1981.

53. Whittley, D. C., and Koenig, D. G., "Large Scale Model Tests of a New Technology V/STOL Concept." AIAA Paper 80-0233, 1980.

54. Garland, D. B., and Whittley, D. C., "Phase I and Wind Tunnel Tests of the J-97 Powered, External Augmentor V/STOL Model." NASA CR-152255, 1980.

55. Garland, D. B., and Harris, J. L., "Phase 2 and 3 Wind Tunnel Tests of the J-97 Powered, External Augmentor V/STOL Model." NASA CR-152380, 1980.

56. Alperin, Morton, and Wu, J. J., "Recent Development of a Jet Diffuser Ejector." AIAA Paper 80-0231, 1980.

57. Alperin, Morton, and Wu, J. J., "A Jet-Diffuser Ejector for a V/STOL Fighter." NASA CR-166161, 1981.

## 7. ACKNOWLEDGMENTS

TABLE 1. GEOMETRY OF GENERAL DYNAMICS E205 MODEL

| Property | Wing | Horizontal canard (midposition) | Vertical tail |
|---|---|---|---|
| Airfoil | | | |
|   Root | NACA 64A204 | NACA 64A005 | 5.3% biconvex |
|   Tip | NACA 64A204 | NACA 64A003 | 4.0% biconvex |
| MAC, m (in.) | 0.340 (13.40) | 0.183 (7.20) | 0.184 (7.26) |
| Aspect ratio | 3.62 | 1.08[a] | 1.27 |
| Taper ratio | 0.190 | 0.37 | 0.43 |
| Root chord, m (in.) | 0.495 (19.51) | 0.249 (9.82) | 0.245 (9.64) |
| Tip chord, m (in.) | 0.094 (3.71) | 0.092 (3.63) | 0.105 (4.14) |
| Span, m (in.) | 1.067 (42.01) | 0.184 (7.26)[a] | 0.222 (8.75) |
| Dihedral, deg | 0 | 0 | --- |
| Incidence, deg | 0 | --- | --- |
| Twist (positive LE up at tip), deg | 0 | 0 | 0 |
| Hinge line | | | |
|   B.L., m (in.) | --- | 0.228 (9.00) | 0 |
|   F.S., m (in.) (coincident with 0.25 MAC) | --- | 0.620 (24.41) | 1.252 (49.30) |
|   W.L., m (in.) | --- | 0.396 (15.59) | 0.403 (15.87) |
| Hinge-line sweep, deg | --- | 1.8 | 0 |
| Leading-edge sweep, deg | 40 | 45 | 47.5 |
| Exposed area, m$^2$ (ft$^2$) | 0.128 (1.374) | 0.029 (0.308)[a] | 0.039 (0.419) |

Wing to centerline ref. area: 0.315 m$^2$ (3.39 ft$^2$)
Total planform ref. area: 0.671 m$^2$ (7.22 ft$^2$)
Body length: 153 m (60.10 in.)

[a]One panel.


Table 2. GEOMETRY OF NORTHROP HATOL MODEL

| Property | Wing | Horizontal canard | Vertical tail |
|---|---|---|---|
| Airfoil | | | |
|   Root | NACA 65A204 | NACA 64A004 | NACA 64A004 |
|   Tip | NACA 64A204 | NACA 64A004 | NACA 65A004 |
| MAC, m (in.) | 0.516 (20.33) | 0.176 (6.91) | 0.141 (5.56) |
| Aspect ratio | 2.12 | 0.77[a] | 1.31[a] |
| Taper ratio | 0.18 | 0.27 | 0.31 |
| Root chord, m (in.) | 0.754 (29.68) | 0.248 (9.79) | 0.198 (7.79) |
| Tip chord, m (in.) | 0.136 (5.34) | 0.068 (2.66) | 0.060 (2.38) |
| Span, m (in.) | 0.943 (37.14) | 0.122 (4.79)[a] | 0.169 (6.65) |
| Dihedral, deg | -3 | 5 | --- |
| Incidence, deg | -0 | --- | --- |
| Twist (positive LE up at tip), deg | -6 | 0 | 0 |
| Hinge line | | | |
|   B.L., m (in.) | --- | 0.128 (5.05) | 0.163 (6.42) |
|   F.S., m (in.) (coincident with 0.25 MAC) | --- | 0.654 (25.75) | 1.42 (55.82) |
|   W.L., m (in.) | --- | 0.053 (2.08) | 0.061 (2.40) |
| Hinge-line sweep, deg | --- | 0 | 0 |
| Leading-edge sweep, deg | 50 | 60 | 42.5 |
| Exposed area, m$^2$ (ft$^2$) | 0.269 (2.90) | 0.019 (0.206)[a] | 0.022 (0.235)[a] |

Wing to centerline ref. area: 0.419 m$^2$ (4.51 ft$^2$)
Total planform ref. area: 0.573 m$^2$ (6.17 ft$^2$)
Body length: 1.52 m (59.84 in.)

[a]One panel.

TABLE 3.  GEOMETRY OF NORTHROP VATOL MODEL

| Property | Wing | Vertical tail |
|---|---|---|
| Airfoil | | |
|   Root | NACA 65A204 | NACA 65A004 |
|   Tip | NACA 64A204 | NACA 64A004 |
| MAC, m (in.) | 0.516 (20.33) | 0.155 (6.12) |
| Aspect ratio | 2.12 | 1.10 |
| Taper ratio | 0.18 | 0.34 |
| Root chord, m (in.) | 0.754 (29.68) | 0.215 (8.46) |
| Tip chord, m (in.) | 0.136 (5.34) | 0.072 (2.85) |
| Span, m (in.) | 0.943 (37.14) | 0.158 (6.22) |
| Dihedral, deg | -3 | --- |
| Incidence, deg | -0 | --- |
| Twist (positive LE up at tip), deg | -6 | 0 |
| Hinge line | | |
|   B.L., m (in.) | --- | 0 |
|   F.S., m (in.) (coincident with 0.25 MAC) | --- | 1.273 (50.11) |
|   W.L., m (in.) | --- | 0.054 (2.12) |
| Hinge-line sweep, deg | --- | 2.5 |
| Leading-edge sweep, deg | 50 | 50 |
| Exposed area, m$^2$ (ft$^2$) | 0.294 (3.16) | 0.023 (0.244) |

Wing to centerline ref. area:  0.419 m$^2$ (4.51 ft$^2$)
Total planform ref. area:  0.545 m$^2$ (5.87 ft$^2$)
Body length:  1.50 m (58.91 in.)

TABLE 4.  GEOMETRY OF GENERAL DYNAMICS E7 MODEL

| Property | Wing | Vertical tail |
|---|---|---|
| Airfoil | | |
|   Root | NACA 0004-63 (optimum supersonic camber — CL = 0.2 @ M = 1.6, C.P. @ 0.511 MAC) | 5.3% biconvex |
|   Tip | NACA 0004-63 | 3.0% biconvex |
| MAC, m (in.) | 0.7978 (31.409) | 0.2315 (9.116) |
| Aspect ratio | 1.665 | 1.294 |
| Taper ratio | 0.115 | 0.437 |
| Root chord, m (in.) | 1.1827 (46.564) | 0.3066 (12.069) |
| Tip chord, m (in.) | 0.1357 (5.342) | 0.1341 (5.278) |
| Span, m (in.) | 1.0973 (43.200) | 0.2850 (11.222) |
| Dihedral, deg | 0 | --- |
| Incidence, deg | 0 | --- |
| Twist (positive LE up at tip), deg | -5.7 | --- |
| Leading-edge sweep, deg | 60 | 47.5 |
| Trailing-edge sweep, deg | -10 | 25.9 |

Wing to centerline reference area:  0.7233 m$^2$ (7.786 ft$^2$)
Body length:  1.579 m (62.718 in.)

TABLE 5. GEOMETRY OF McDONNELL DOUGLAS 279-3 MODEL

| Property | Wing (theoretical) | Canard (exposed) | Horizontal tail (exposed) | Vertical tail |
|---|---|---|---|---|
| Airfoil | | | | |
|   Root | 64AX06.2 MOD | 64A008 | 64A008 | 64A005 |
|   Tip | 64AX04 MOD | 64A003 | 64A003 | 64A003 |
| MAC, m (in.) | 0.3751 (14.768) | 0.1678 (6.607) | 0.1678 (6.607) | 0.2223 (8.753) |
| Aspect ratio | 3.00 | 3.00 | 3.00 | 1.20 |
| Taper ratio | 0.25 | 0.25 | 0.25 | 0.35 |
| Root chord, m (in.) | 0.5361 (21.108) | 0.2397 (9.438) | 0.2397 (9.438) | 0.3057 (12.037) |
| Tip chord, m (in.) | 0.1340 (5.277) | 0.0599 (2.359) | 0.0599 (2.359) | 0.1070 (4.214) |
| Span, m (in.) | 1.0049 (39.564) | 0.4493 (17.688) | 0.4493 (17.688) | 0.2478 (9.756) |
| Dihedral, deg | -9 | 0 | 0 | --- |
| Incidence, deg | 0 | 0 | 0 | --- |
| Twist (positive LE up at tip), deg | -4 | 0 | 0 | --- |
| Hinge line | | | | |
|   B.L., m (in.) | --- | 0.1072 (4.220) | 0.0386 (1.520) | --- |
|   F.S., m (in.) (coincident with 0.25 MAC) | --- | 0.4984 (19.624) | 1.3642 (53.708) | --- |
|   W.L., m (in.) | --- | 0.2734 (10.764) | 0.2464 (9.700) | --- |
| Hinge line sweep, deg | --- | 0 | 0 | --- |
| Leading-edge sweep, deg | 45 | 50 | 50 | 45 |
| Trailing-edge sweep, deg | 11.3 (avg.) | 21.4 | 21.4 | 11.2 |
| Exposed area, $m^2$ ($ft^2$) | --- | 0.0674 (0.725) | 0.0674 (0.725) | 0.0511 (0.550) |

Wing to centerline reference area: 0.3369 $m^2$ (3.626 $ft^2$)
Body length: 1.5486 m (60.968 in.)
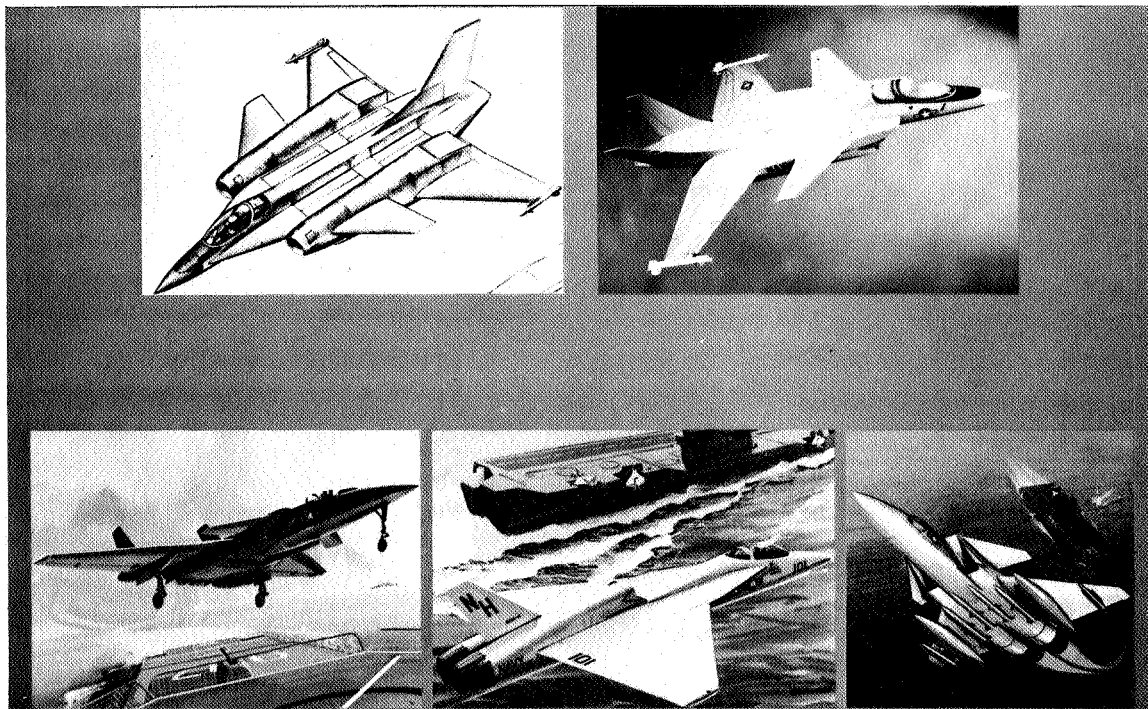
Figure 1. Twin-engine V/STOL fighter concepts.
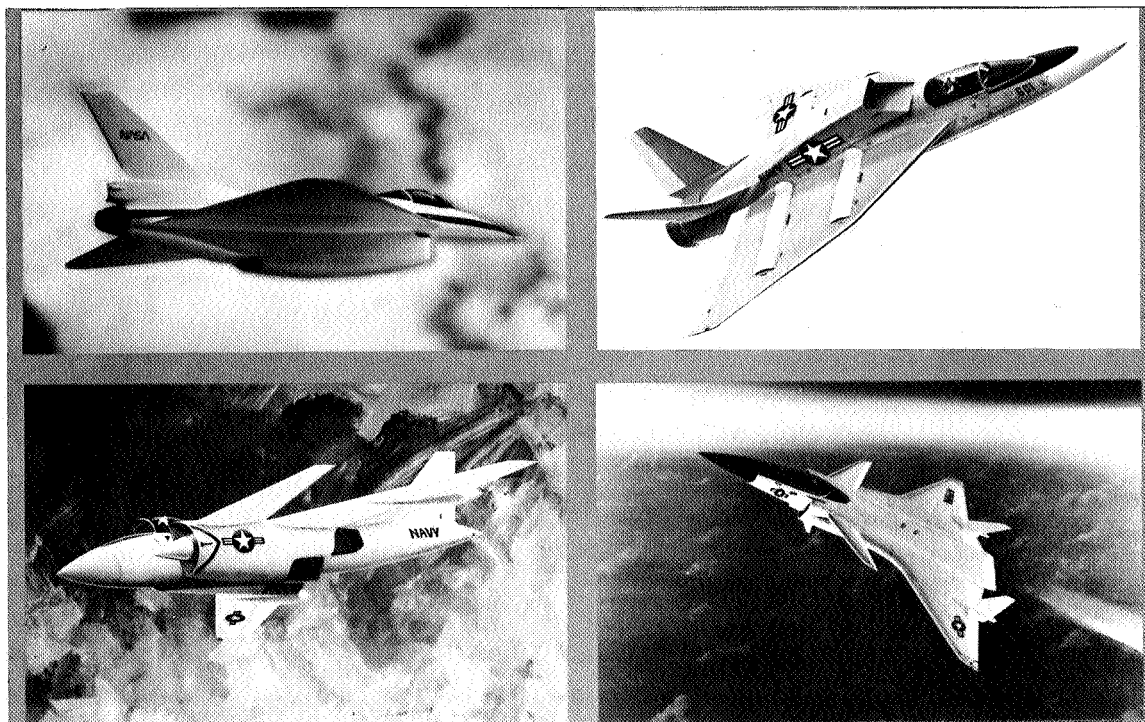


Figure 2. Single-engine V/STOL and STOVL fighter concepts.
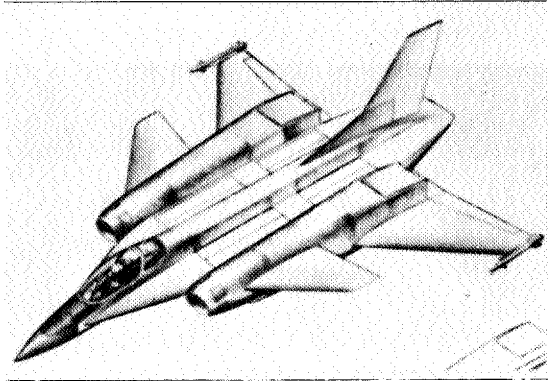
AERODYNAMIC UNCERTAINTIES

- MINIMUM DRAG
- A.C. LOCATION
- $C_{L_{max}}$ USABLE
- BUFFET ONSET
- LATERAL/DIRECTIONAL CHARACTERISTICS
- SUPERCIRCULATION
- WIDE-BODY CONFIGURATION AERODYNAMICS

Figure 3. Aerodynamic uncertainties of General Dynamics twin-engine concept.
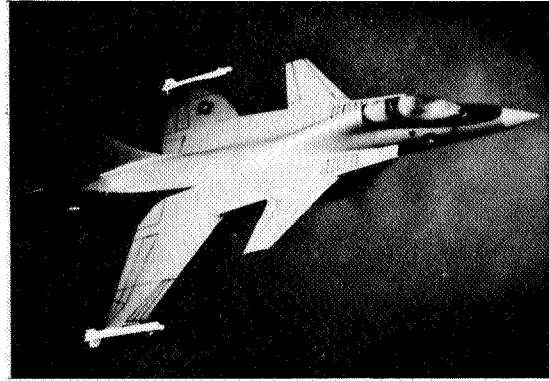


AERODYNAMIC UNCERTAINTIES

- SUPERCRITICAL, MULTI-ELEMENT WING AERODYNAMICS
- MINIMUM DRAG
- BUFFET ONSET
- WIDE-BODY CONFIGURATION AERODYNAMICS
- WING/CANARD INTERACTIONS
- HIGH $\alpha$ CHARACTERISTICS
- THRUST VECTORING/SUPERCIRCULATION

Figure 4. Aerodynamic uncertainties of Grumman twin-engine concept.
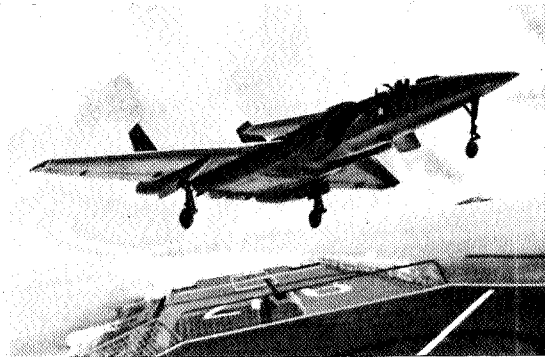


AERODYNAMIC UNCERTAINTIES

- MINIMUM DRAG
- CANARD EFFECT ON STABILITY AND A.C. LOCATION
- CANARD/WING FLAP COMBINATION FOR MINIMUM $C_{D_L}$
- CANARD EFFECT ON DIRECTIONAL CHARACTERISTICS
- TWIN AFTERBODY DRAG
- VECTORED THRUST FOR MANEUVER

Figure 5. Aerodynamic uncertainties of Northrop HATOL twin-engine concept.
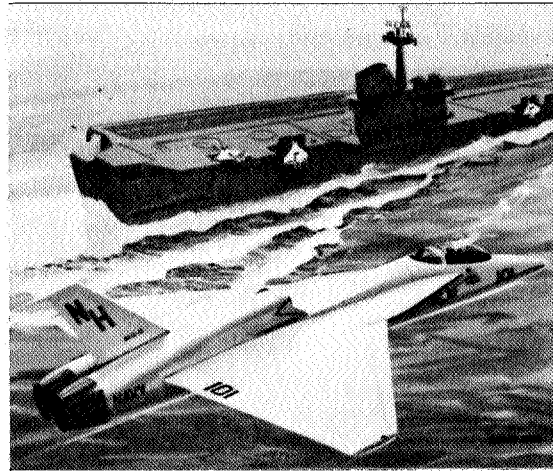


AERODYNAMIC UNCERTAINTIES

- MINIMUM DRAG
- LEX EFFECT AT HIGH $\alpha$
- A.C. TRAVEL
- MANEUVER FLAPS FOR DRAG IMPROVEMENT AT M > 1
- TOP INLETS
- BUFFET ONSET
- INLET SPILLAGE EFFECTS

Figure 6. Aerodynamic uncertainties of Northrop VATOL twin-engine concept.
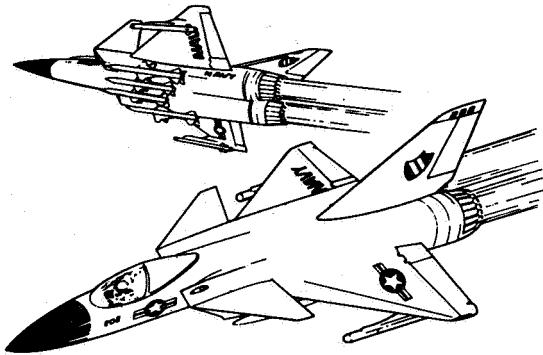
AERODYNAMIC UNCERTAINTIES

- TRANSITION AERODYNAMICS
- MINIMUM DRAG AND DRAG RISE
- VARIABLE CAMBER WING
- BUFFET ONSET
- WING/CANARD INTERACTIONS
- INLETS AT EXTREME $\alpha$ AND $\beta$

Figure 7. Aerodynamic uncertainties of Vought twin-engine concept.
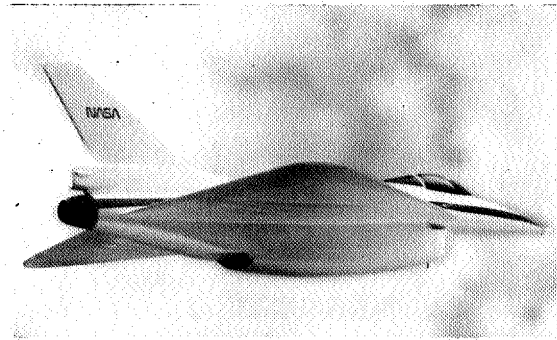


AERODYNAMIC UNCERTAINTIES

- LATERAL/DIRECTIONAL CHARACTERISTICS
- WING CAMBER RESTRICTED BY EJECTOR
- WING PLANFORM EFFECTS
- AERODYNAMIC/EJECTOR INTERACTIONS
- TAILLESS CONFIGURATION AERODYNAMICS
- 2-D NOZZLE/FUSELAGE INTEGRATION
- MINIMUM DRAG

Figure 8. Aerodynamic uncertainties of General Dynamics single-engine concept.
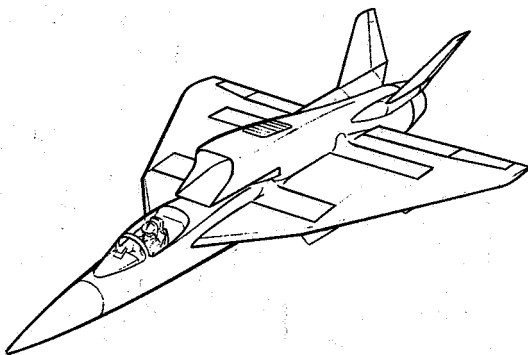


AERODYNAMIC UNCERTAINTIES

- MINIMUM DRAG
- DRAG DUE TO LIFT
- WING PLANFORM EFFECTS
- DRAG OF BLUNT WING TRAILING EDGES
- HIGH ANGLE-OF-ATTACK AERODYNAMICS
- TOP INLET
- WING-TIP MOUNTED VERTICAL TAILS

Figure 9. Aerodynamic uncertainties of Rockwell single-engine concept.
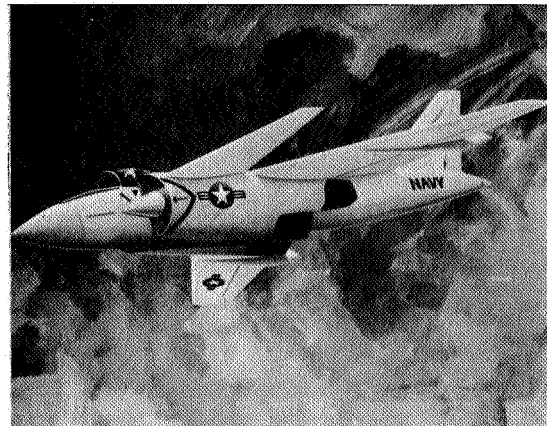


AERODYNAMIC UNCERTAINTIES

- CLOSE-COUPLED CANARD EFFECTS ON:
  - LATERAL/DIRECTIONAL CHARACTERISTICS
  - $C_L$ AND Cm AT HIGH $\alpha$
  - LONGITUDINAL STABILITY
- LARGE HALF-AXISYMMETRIC INLETS
- FORWARD LOCATION OF ENGINE
- MINIMUM DRAG
- PROPULSIVE FLOW EFFECTS ON AERODYNAMICS
- PREDICTION OF CANARD EFFECTS

Figure 10. Aerodynamic uncertainties of McDonnell-Douglas single-engine concept.
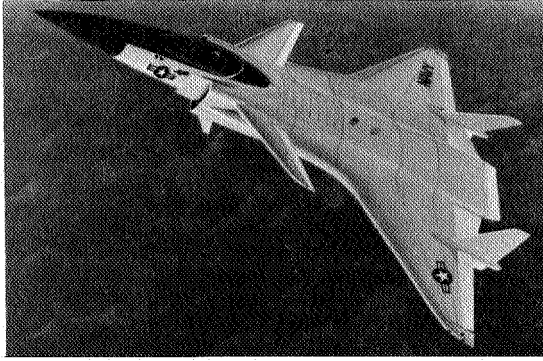
**AERODYNAMIC UNCERTAINTIES**

● **STRAKE AND CANARD EFFECTS**

● **BLENDED WING BODY AERODYNAMICS**

● **MINIMUM DRAG**

● **LATERAL/DIRECTIONAL CHARACTERISTICS**

● **MULTIPLE CONTROL EFFECTIVENESS**

● **FORWARD TWO-AXES CONTROL SURFACE**

● **AERODYNAMIC PREDICTION METHODS**

Figure 11. Aerodynamic uncertainties of Vought single-engine concept.
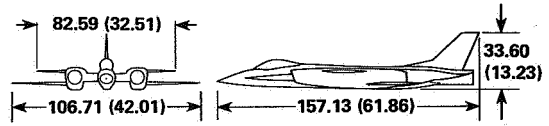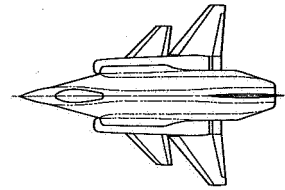


Figure 12. Wind-tunnel model of General Dynamics E205 configuration.
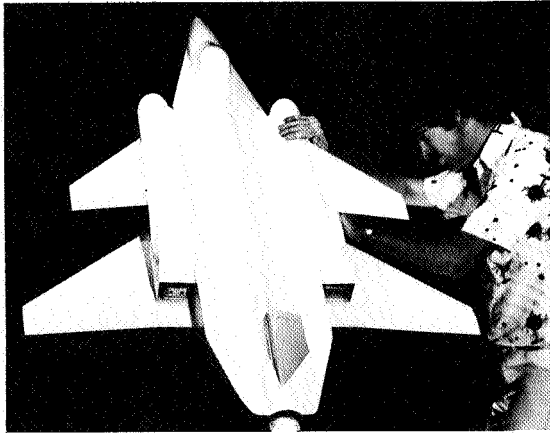


(a)
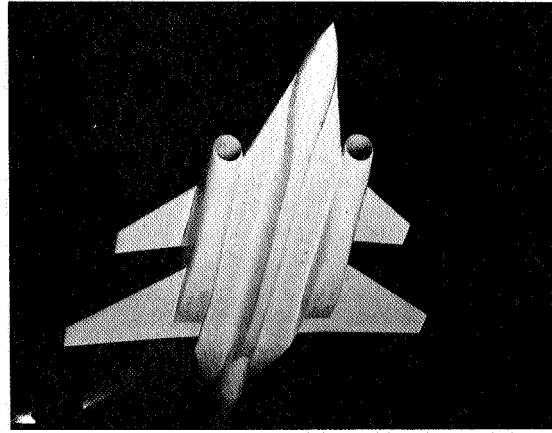


(b)

Figure 13. Model of General Dynamics E205 configuration in Ames 12-Foot Wind Tunnel.
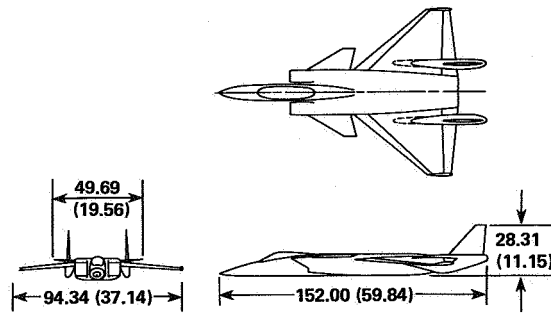


Figure 14. Wind-tunnel model of Northrop HATOL configuration.

(a)
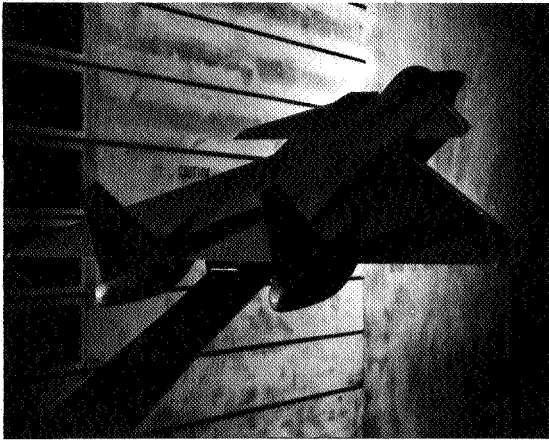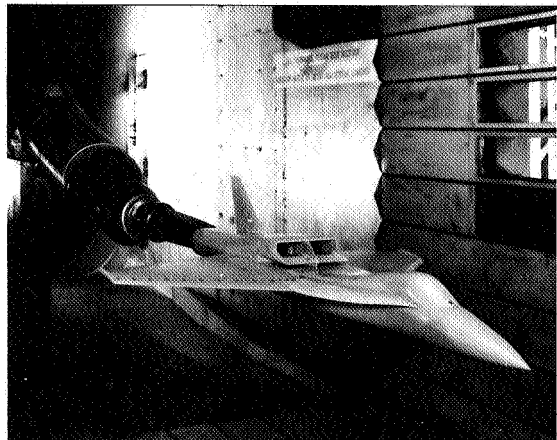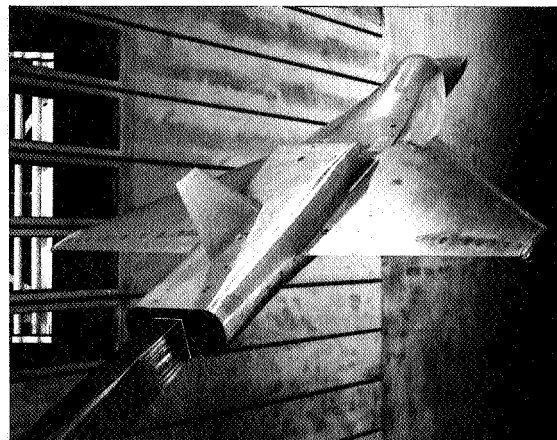


(b)

Figure 15. Model of Northrop HATOL configuration in Ames 11-Foot Wind Tunnel.



(a)



(b)

Figure 17. Model of Northrop VATOL configuration in Ames 11-Foot Wind Tunnel.



STANDARD LEX

ALTERNATE LEX

28.66 (11.28)

94.34 (37.14)

149.63 (58.91)
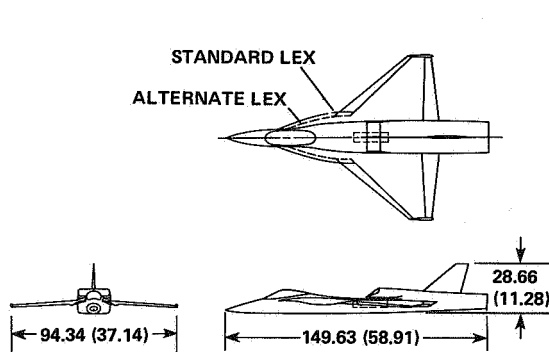
Figure 16. Wind-tunnel model of Northrop VATOL configuration.



109.73 (43.20)

159.31 (62.72)
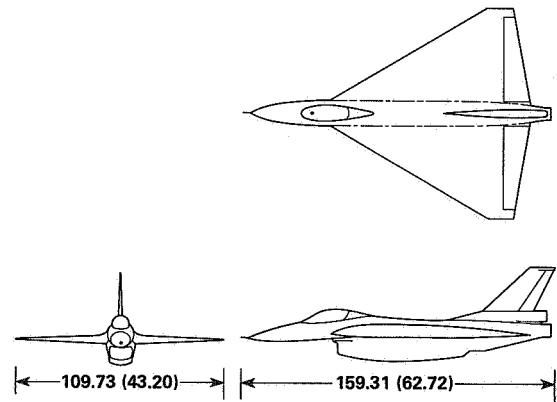
Figure 18. Wind-tunnel model of General Dynamics E7 configuration.

24
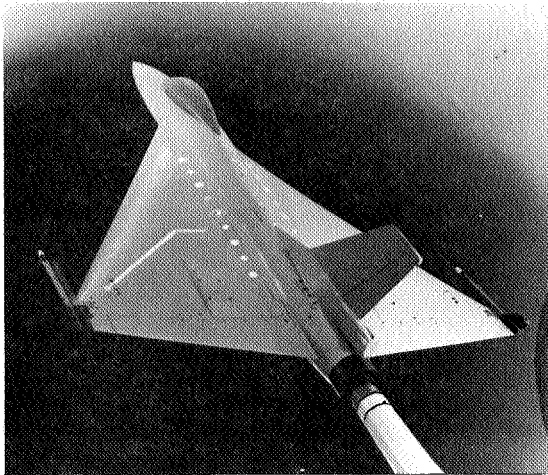

(a)
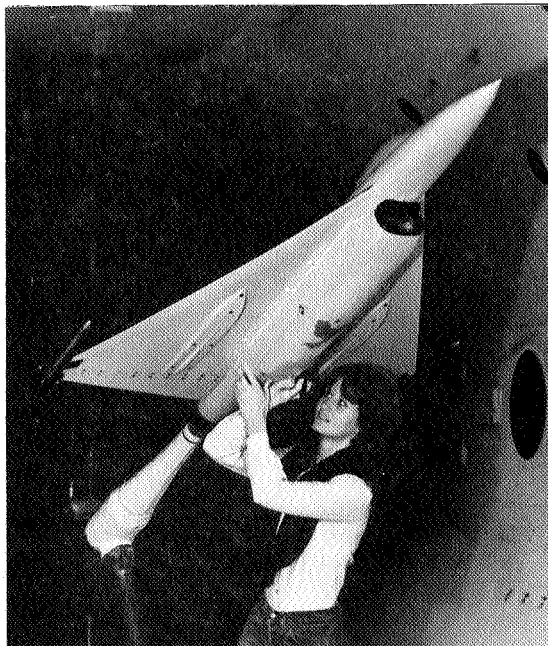

(b)

Figure 19.  Model of General Dynamics E7
configuration in Ames 12-Foot Wind Tunnel.



66.37
(26.13)

40.80
(16.06)

|←—100.49 (39.56)—→|     |←——154.86 (60.97)——→|
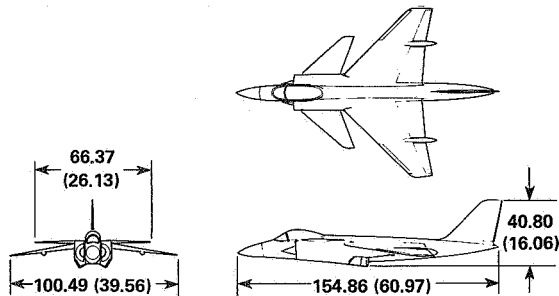
Figure 20.  Wind-tunnel model of McAir 279
configuration.
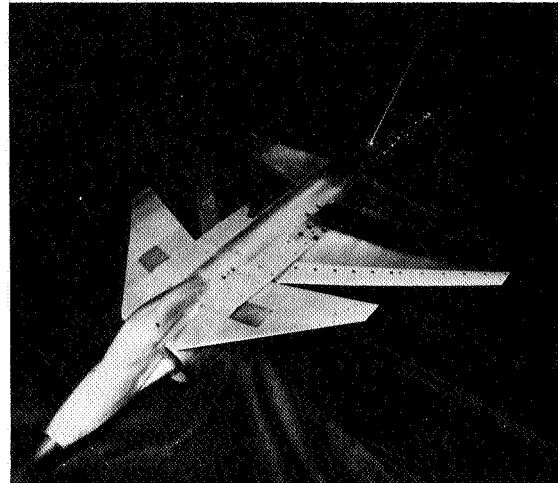


Figure 21.  Model of the McAir 279 deflected thrust
concept (flow-through configuration).



—— ESTIMATED DRAG
O  WIND-TUNNEL DATA
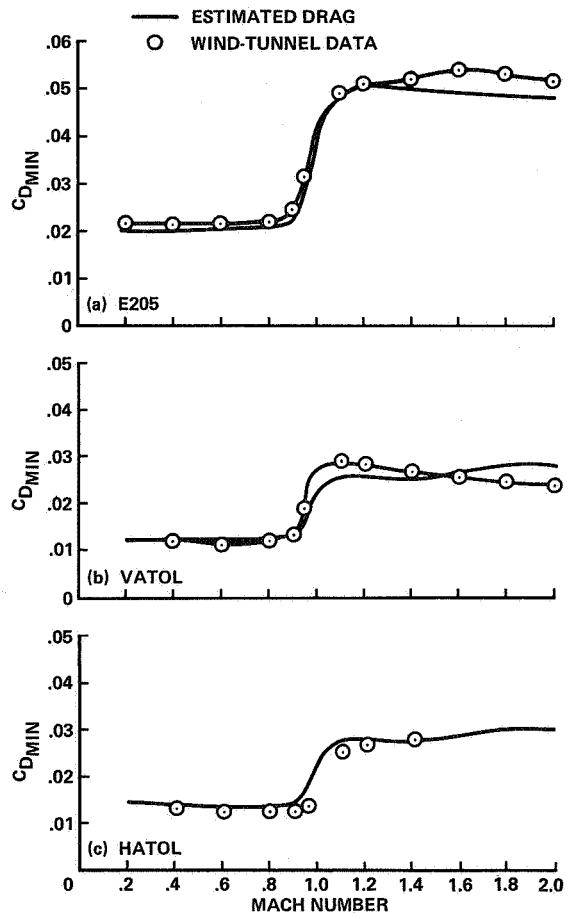
Figure 22.  Minimum drag coefficients for the three
twin-engine models based on wing reference area.

BASELINE CONFIGURATIONS M = 0.6
ORIGINAL REFERENCE AREA:
WING TO FUSELAGE $\mathbb{C}$

| | | REFERENCE AREA, ft$^2$ |
|---|---|---|
| △ | VATOL | 4.51 |
| □ | HATOL | 4.51 |
| ○ | E205 | 3.39 |

REVISED REFERENCE AREA:
TOTAL PLANFORM AREA

| | | REFERENCE AREA, ft$^2$ |
|---|---|---|
| △ | VATOL | 5.87 |
| □ | HATOL | 6.17 |
| ○ | E205 | 7.22 |

Figure 23. Reference area effects.

| | |
|---|---|
| ○ | E205 |
| □ | VATOL |
| △ | HATOL |
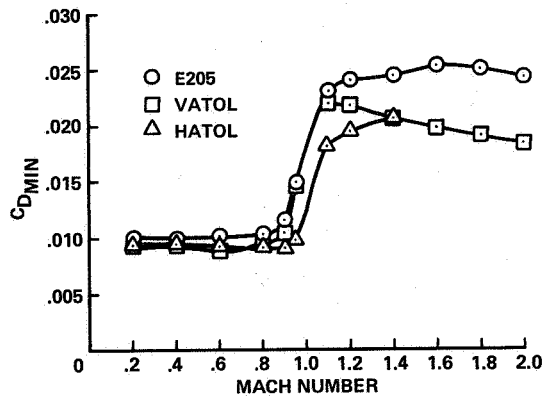
Figure 24. Minimum drag coefficients for the three twin-engine models based on total planform area.

WING + BODY + AFTERBODIES + CANARD + VERTICALS

WING + BODY + AFTERBODIES

WING + BODY

BODY

NOTE: BODY INCLUDES NACELLES

Figure 25. Minimum drag component buildup for the Northrop HATOL model.

OPEN SYMBOLS — EXISTING AIRCRAFT
SOLID SYMBOLS — V/STOL MODELS

$S_F$ = MAXIMUM CROSS SECTION − 0.95 $A_C$
L = OVERALL LENGTH
$\Delta C_{D_p}$ BASED ON $S_F$

2.0 x S.H.

1.5 x S.H.

SEARS-HAACK OPTIMUM BODY OF REVOLUTION
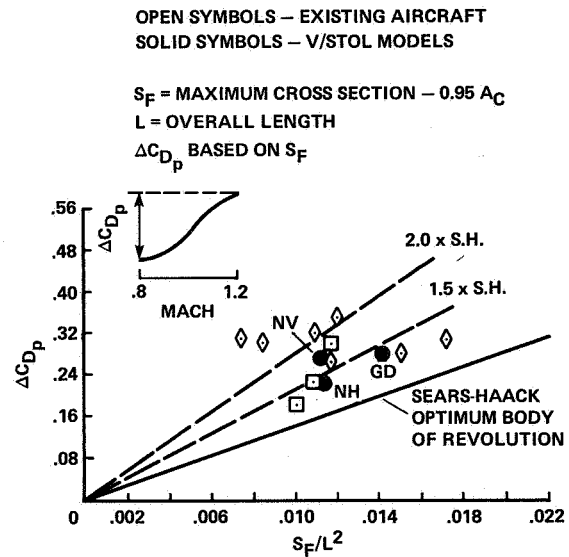
Figure 26. Wave drag comparison.
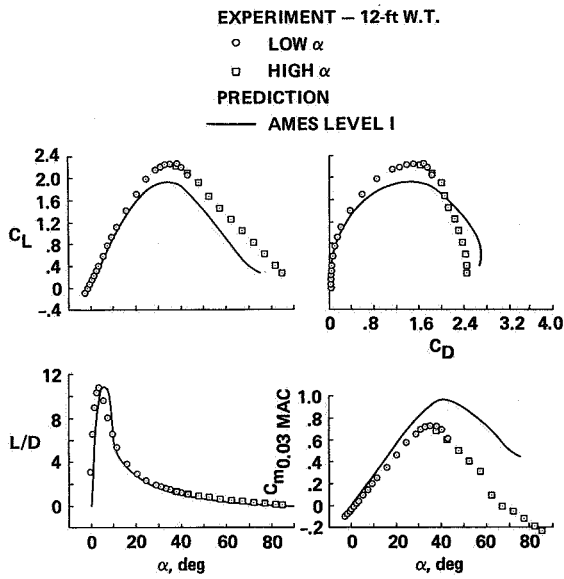
Figure 27. High angle-of-attack characteristics of the E205 model; M = 0.2.
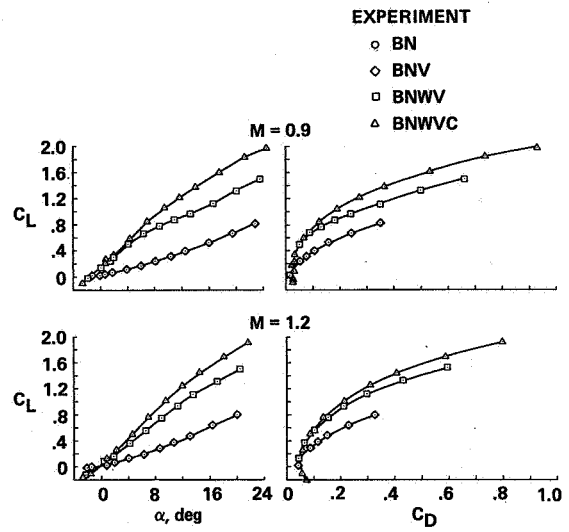


Figure 28. Component buildup for the E205 model.
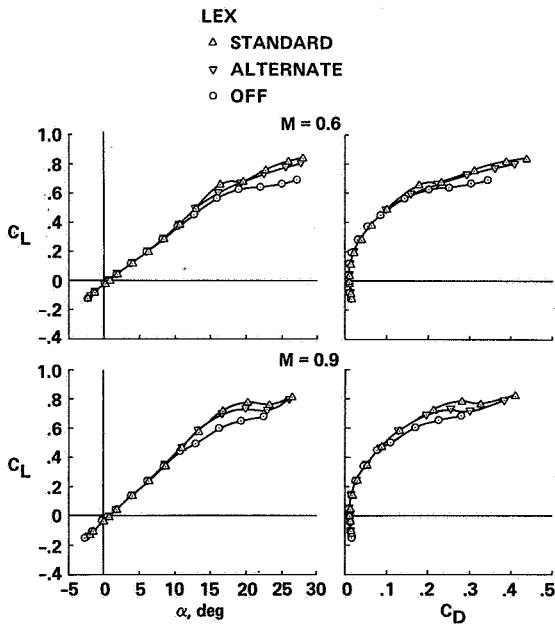


Figure 29. Effect of LEX size on VATOL model; based on total planform area.
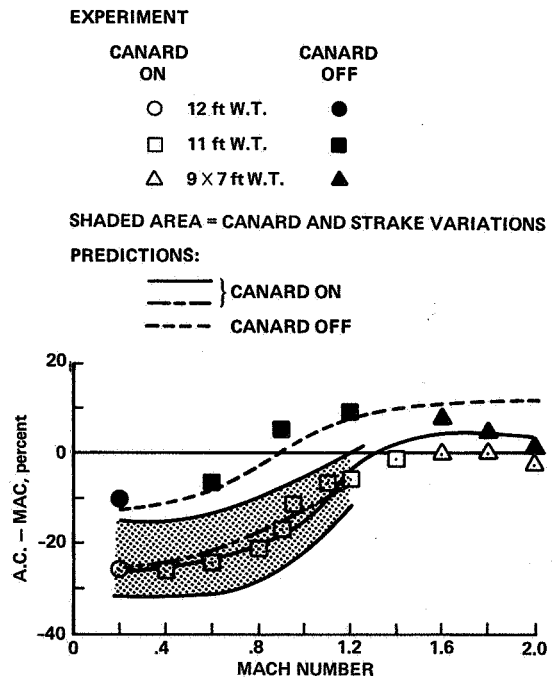


Figure 30. Aerodynamic center location for the E205 model.
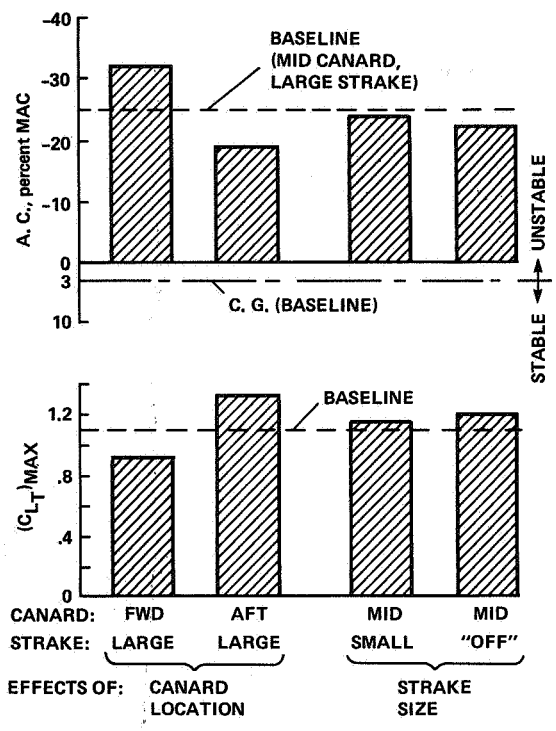
Figure 31. Effects of canard and strake variations on stability and maximum trimmed lift for the E205 model.
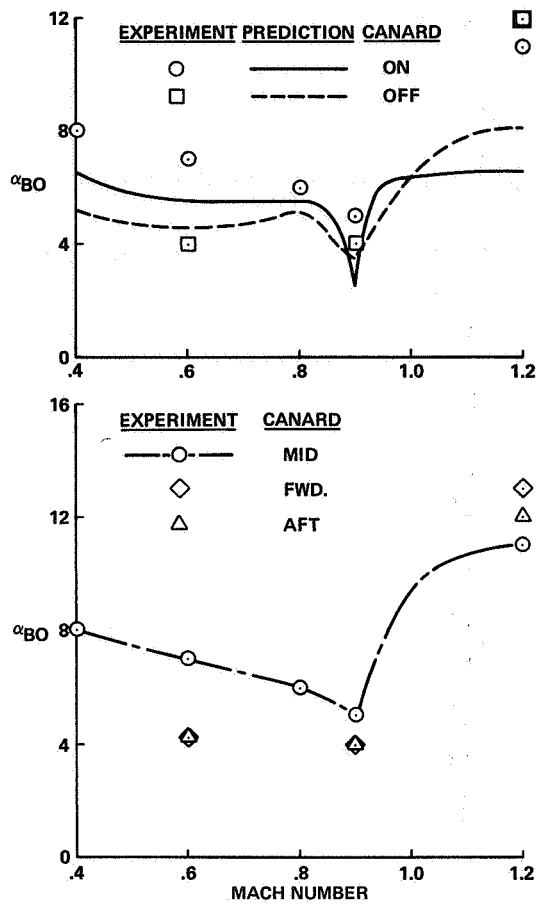


Figure 32. Buffet-onset angle of attack for the E205 model.
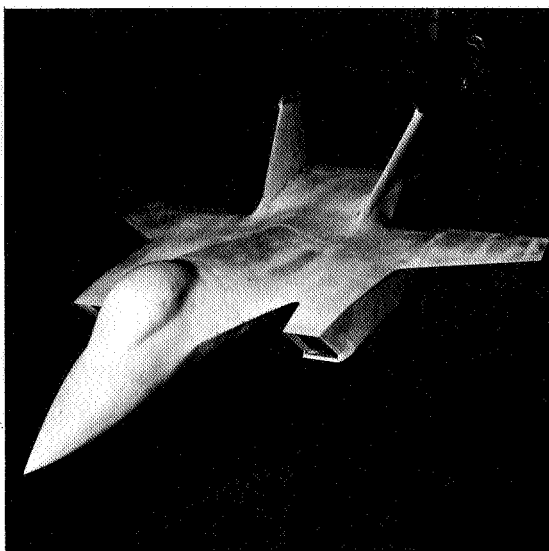


Figure 33. Grumman 623 model installed in the Ames 11-Foot Wind Tunnel.
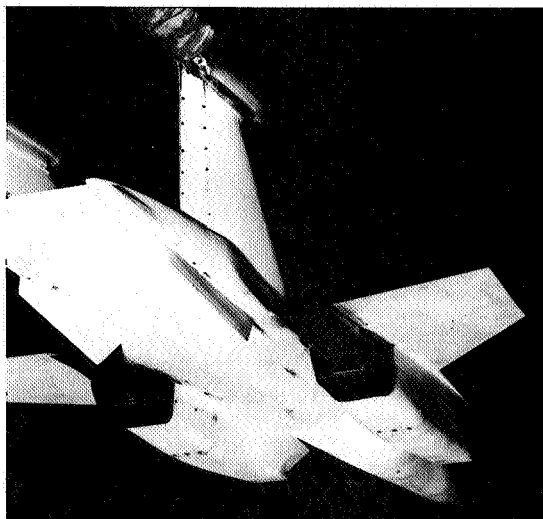


Figure 34. ADEN nozzles on the 623 model.

M = 0.9  NPR = 6.0
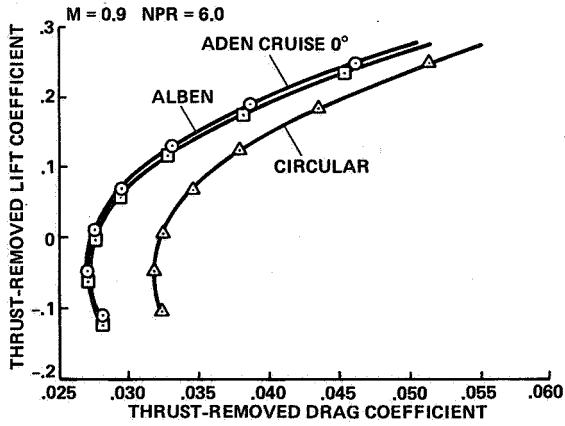
Figure 35.  ADEN, ALBEN, and circular nozzle thrust-removed polar comparison.
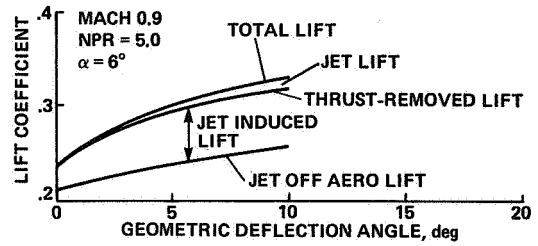
Figure 36.  ADEN cruise lift component buildup.
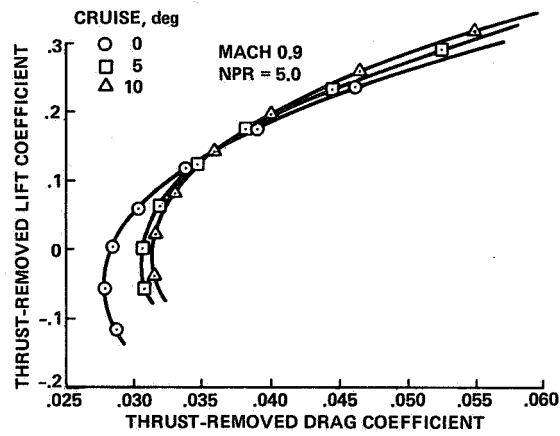
Figure 37.  Effect of ADEN cruise vectoring.
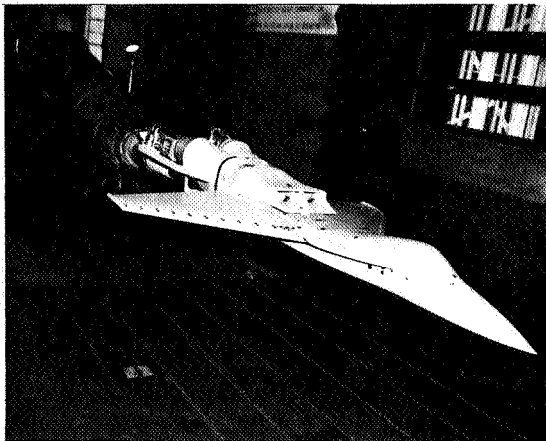
(a)
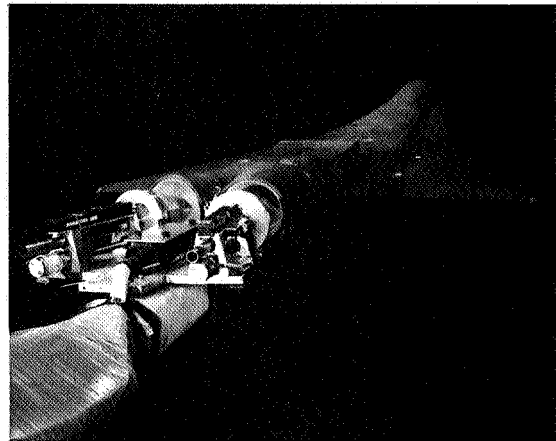
(b)

Figure 38.  Northrop VATOL top inlet model in Ames 11-Foot Wind Tunnel.
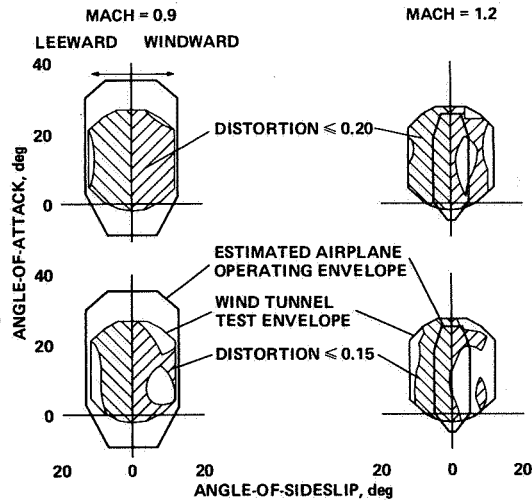
Figure 39.. Distortion-limited operating envelopes for the VATOL configuration.
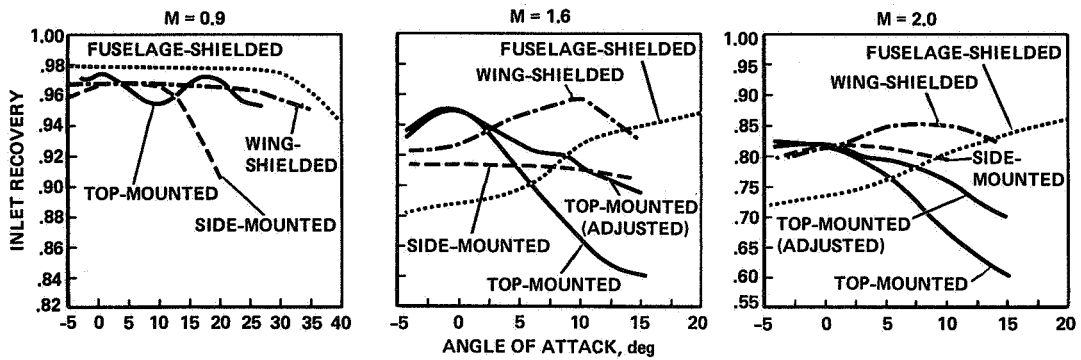


Figure 40. Comparison of inlet recoveries for the top and conventional inlet installations.
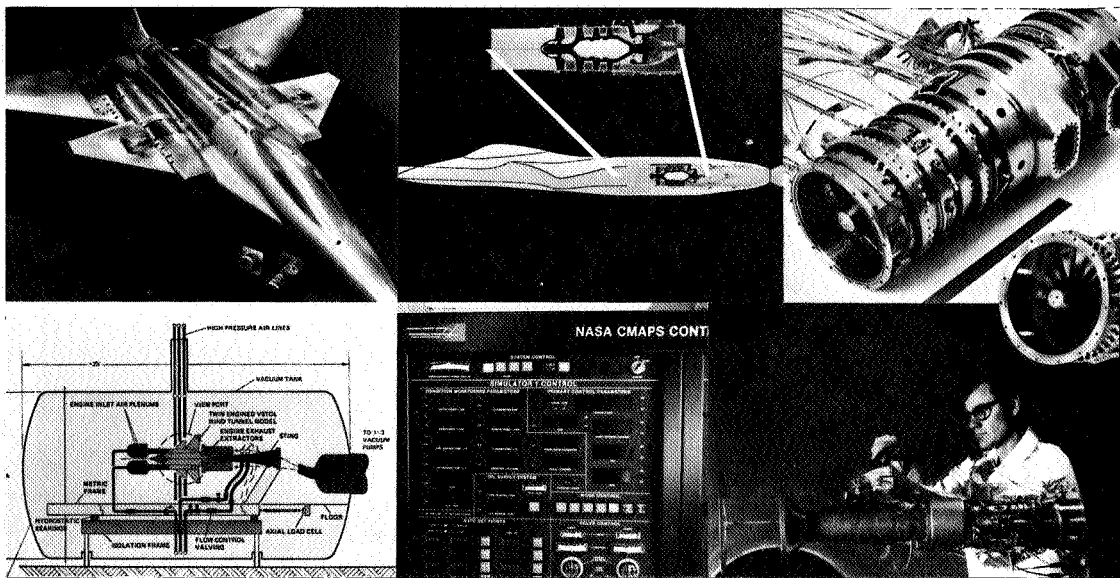


Figure 41. Elements of the propulsion simulator research program.

Figure 42. CMAPS model in Ames 11-Foot Wind Tunnel.
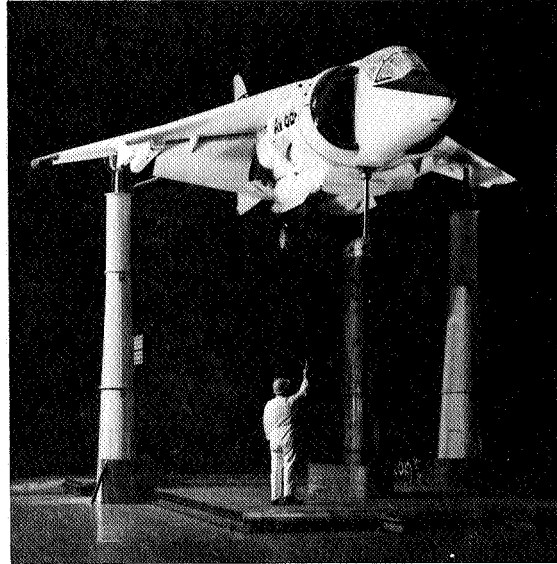


Figure 45. AV-8B in Ames 40- by 80-Foot Wind Tunnel.
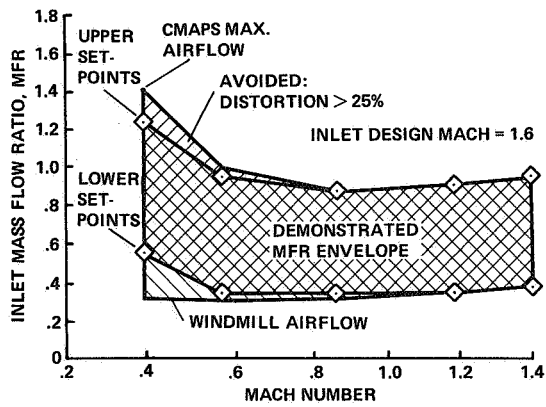


Figure 43. Demonstrated inlet mass flow ratio envelope.
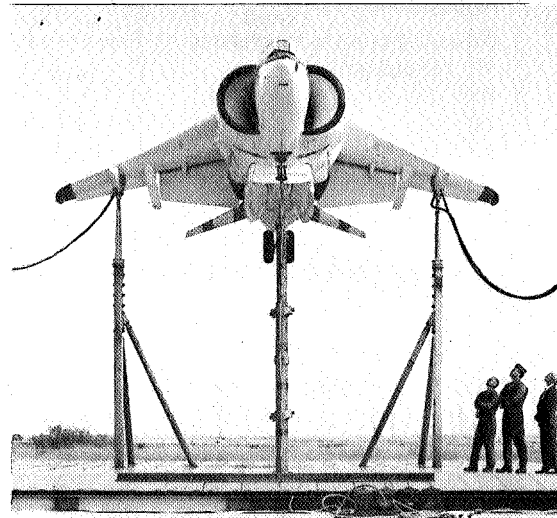


Figure 46. AV-8B on Ames Outdoor Aerodynamic Research Facility.
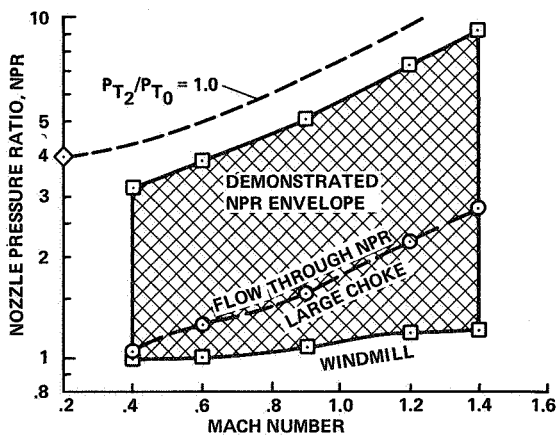


Figure 44. Demonstrated nozzle pressure ratio envelope.
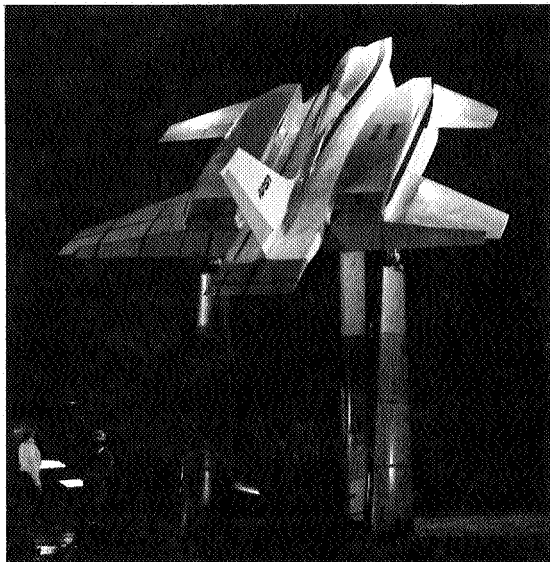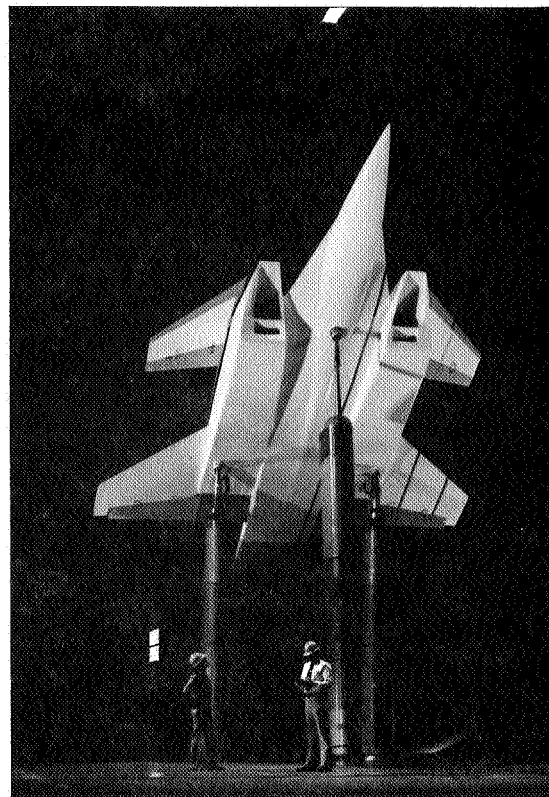
(a)  (b)

Figure 47.  Twin-engine V/STOL fighter model in Ames 40- by 80-Foot Wind Tunnel.



WING:
  REFERENCE AREA, m² (ft²)    16.91 (182)
  ASPECT RATIO                3.13
  TAPER RATIO                 0.243
  AIRFOIL SECTION             64A204
  GEOMETRIC TWIST             4°
  MEAN AERO CHORD, m (ft)     2.61 (8.56)

CANARD:
  AREA, m² (ft²)              3.53 (37.98)
  CANARD AREA/WING AREA       0.208
  ASPECT RATIO                2.07
  TAPER RATIO                 0.419
  AIRFOIL SECTION             64A004
  MEAN AERO CHORD, m (ft)     1.38 (4.52)

ALL DIMENSIONS IN m (ft)
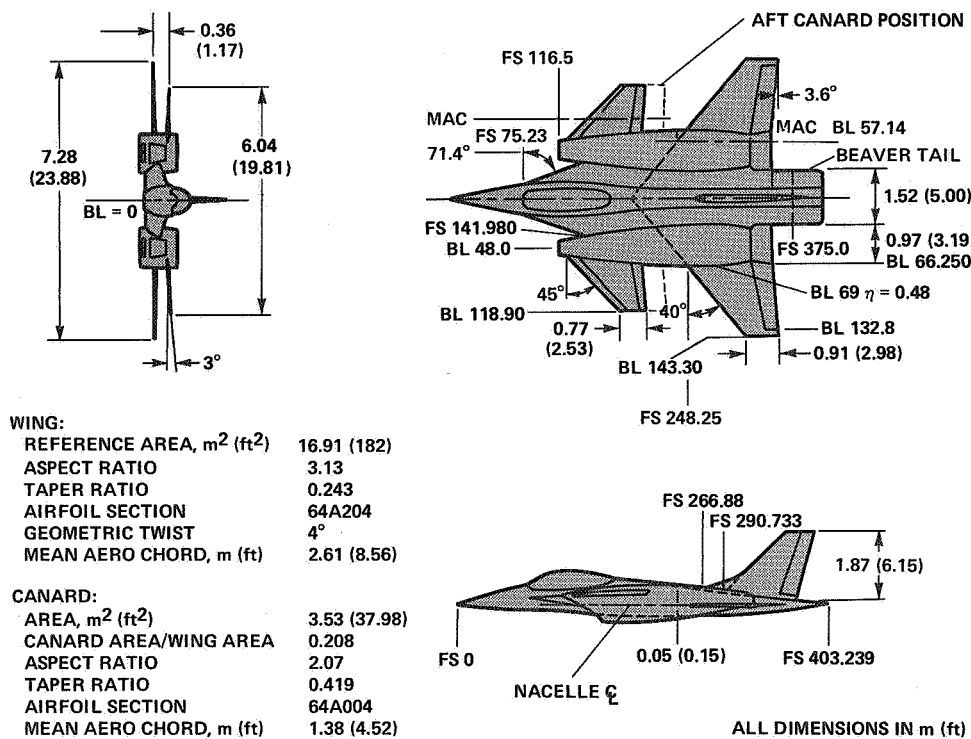
Figure 48.  Twin-engine V/STOL fighter model geometry.
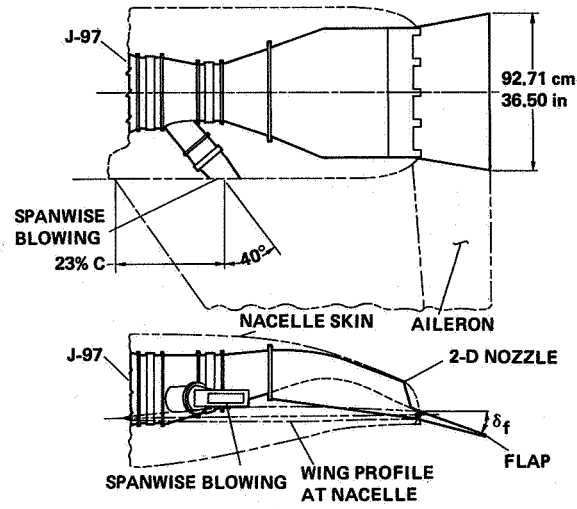
Figure 49. Twin-engine fighter model nozzle geometry.
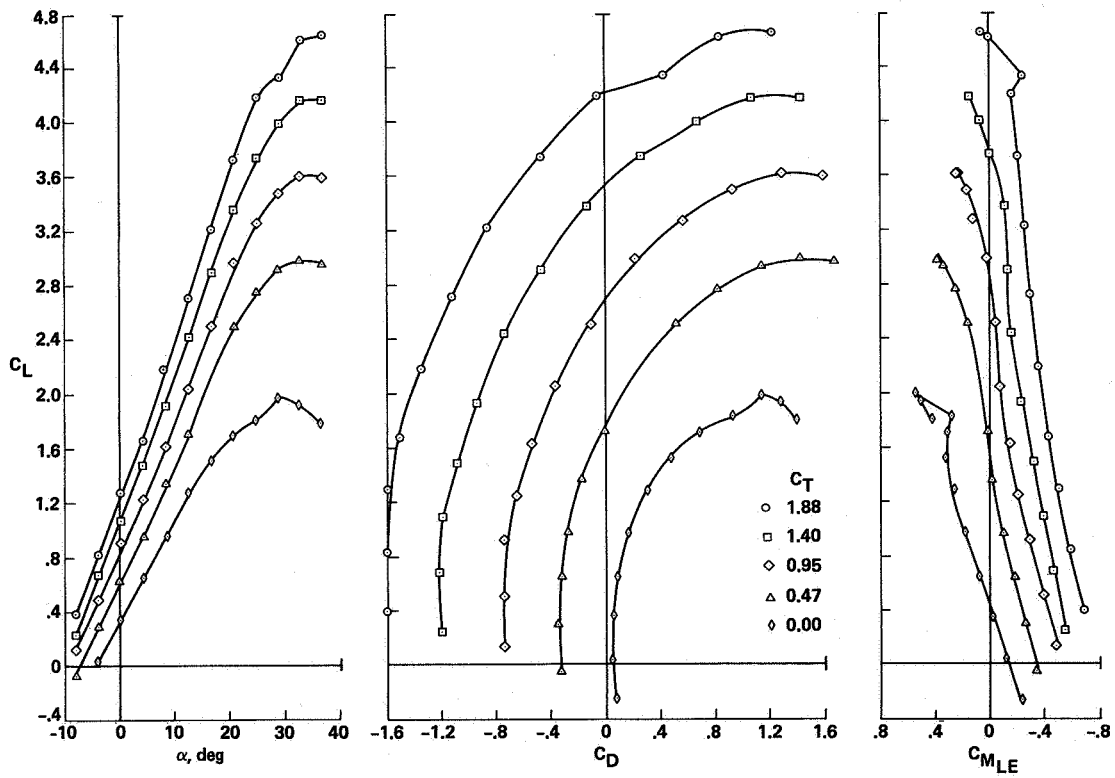


Figure 50. Longitudinal characteristics of the twin-engine fighter model with USB and SWB.
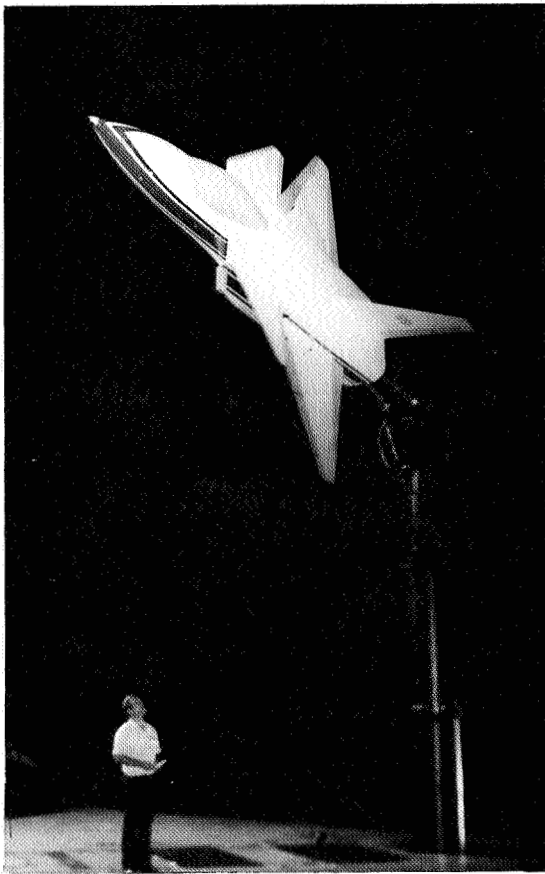
Figure 51. High angle-of-attack installation in the Ames 40- by 80-Foot Wind Tunnel.



1.913
(6.278)

1.451
(4.761)

3.299
(10.823)

5.387 (17.673)
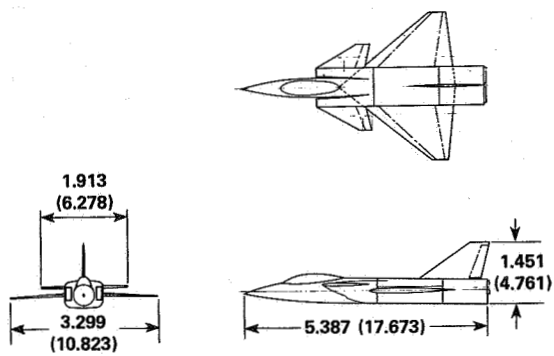
Figure 52. Geometry of the model of the Vought configuration.



TOP VIEW

$V_\infty$

$\alpha_0$

TEST SECTION
TURNTABLE

SIDE VIEW

$V_\infty$

$\beta_0$

FLOOR
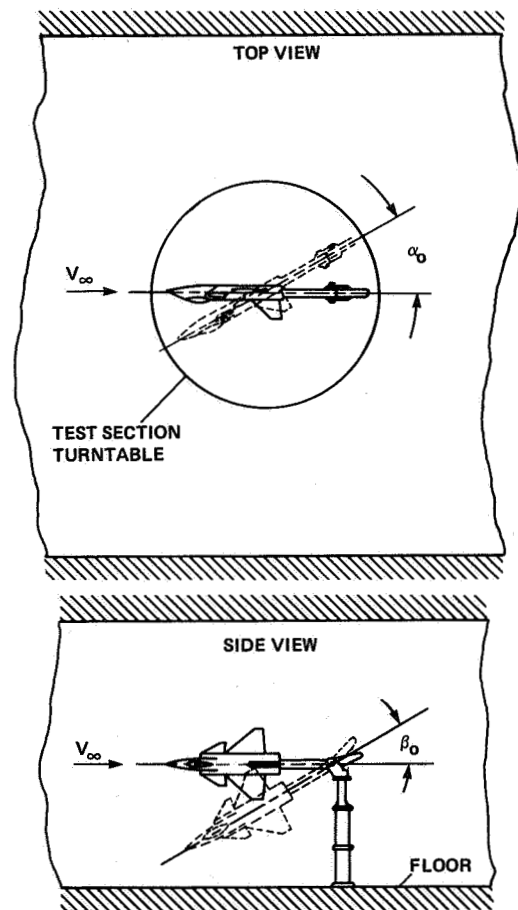
Figure 53. Pitch and yaw methods for high angle-of-attack testing in the Ames 40- by 80-Foot Wind Tunnel.

34
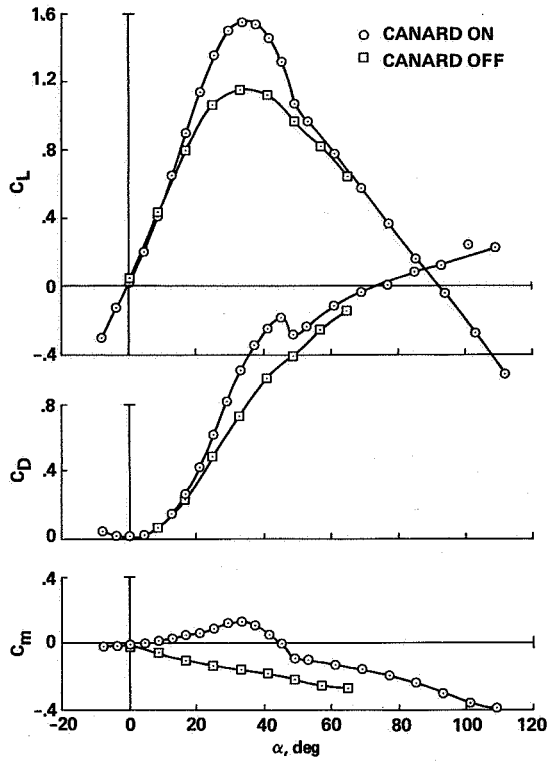


Figure 54. Low-speed, high angle-of-attack characteristics of the Vought model.
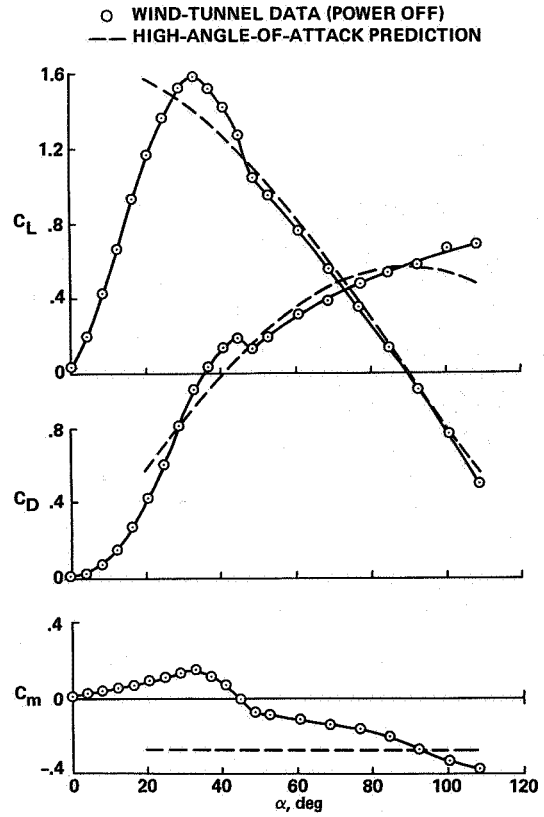
Figure 55. Prediction of high angle-of-attack characteristics of the Vought model.



(a) FUSELAGE EJECTOR

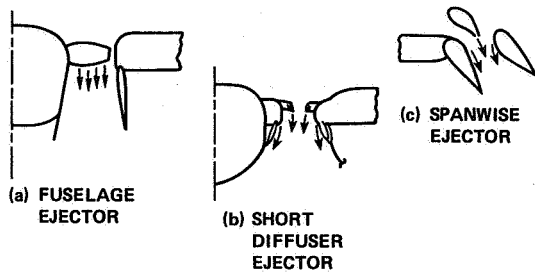(b) SHORT DIFFUSER EJECTOR

(c) SPANWISE EJECTOR

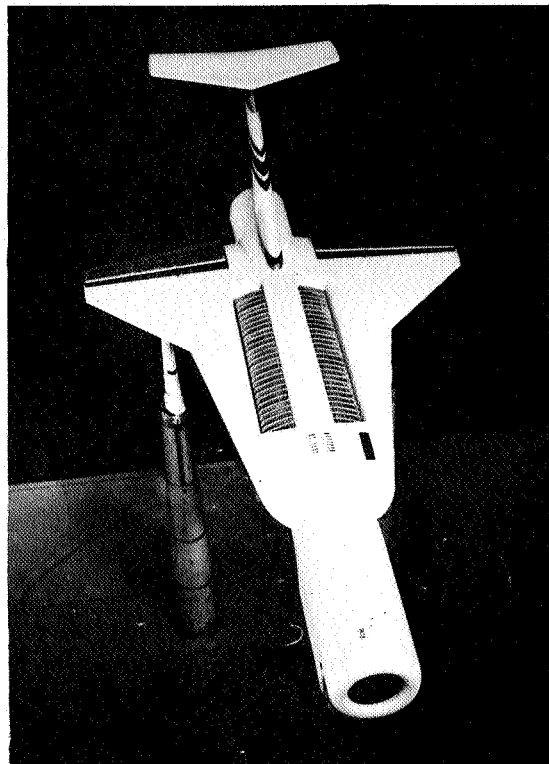Figure 56. Thrusting ejector concepts for V/STOL aircraft having "V" capability.



Figure 57. J97 powered ejector model in the Ames 40- by 80-Foot Wind Tunnel.
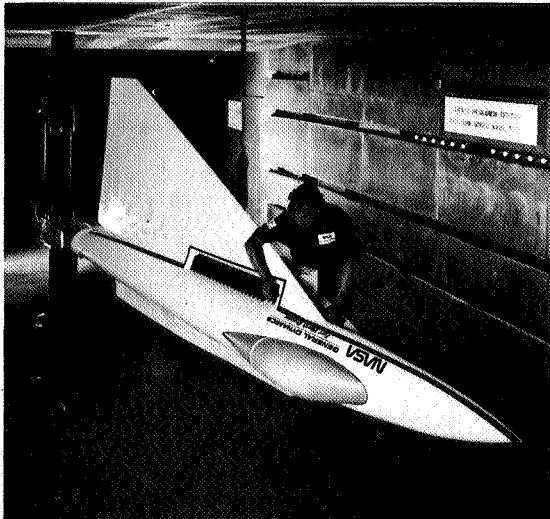
Figure 58.  One-third-scale, powered ejector model of the E7 configuration in the Lewis 9- by 15-Foot Wind Tunnel.
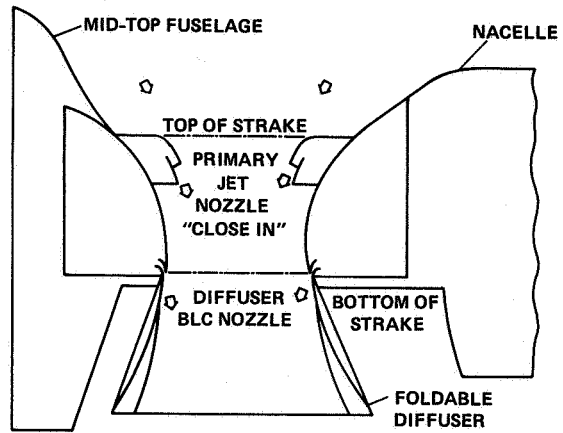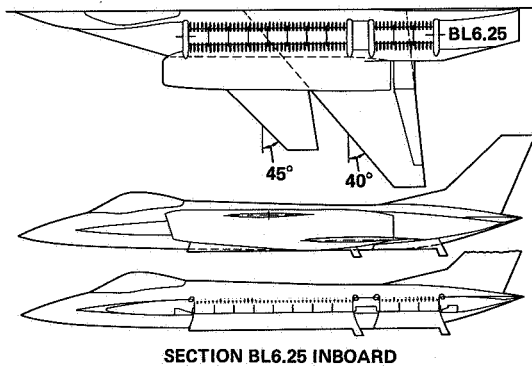


Figure 59.  Short diffuser ejector.



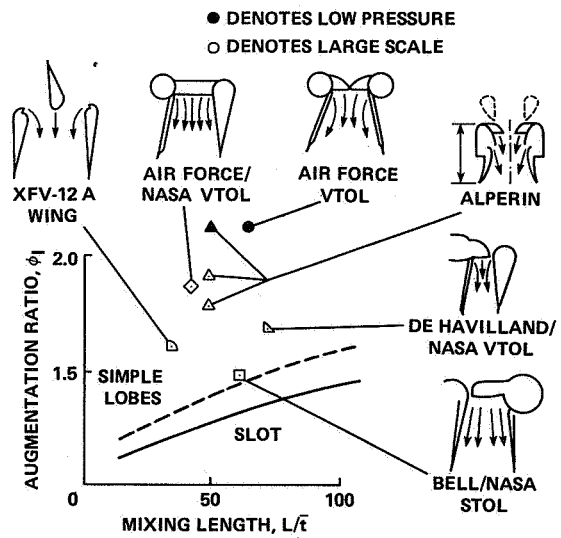Figure 60.  E205 semispan ejector model.



Figure 61.  Summary of lift augmenting ejector performance.

| 1. Report No. NASA TM-85937 | 2. Government Accession No. | 3. Recipient's Catalog No. |
|---|---|---|

| 4. Title and Subtitle | 5. Report Date |
|---|---|
| ASSESSMENT OF AERODYNAMIC PERFORMANCE OF V/STOL AND STOVL FIGHTER AIRCRAFT | April 1984 |
| | 6. Performing Organization Code |

| 7. Author(s) | 8. Performing Organization Report No. |
|---|---|
| W. P. Nelms | A-9690 |

| | 10. Work Unit No. |
|---|---|
| | T-3288Y |

| 9. Performing Organization Name and Address | 11. Contract or Grant No. |
|---|---|
| Ames Research Center Moffett Field, CA 94035 | |

| | 13. Type of Report and Period Covered |
|---|---|
| 12. Sponsoring Agency Name and Address | Technical Memorandum |
| National Aeronautics and Space Administration Washington, DC 20546 | 14. Sponsoring Agency Code |
| | 505-43-01 |

15. Supplementary Notes

Point of Contact: W. P. Nelms, Ames Research Center, MS 227-2, Moffett Field, CA 94035 (415) 965-5879 or FTS 448-5879

16. Abstract

This paper summarizes research efforts in the United States to assess the aerodynamic performance of V/STOL and STOVL fighter/attack aircraft. Emphasis is on research programs at NASA Ames Research Center conducted jointly with DOD and the Industry. Aerodynamic and propulsion/airframe integration activities are described considering both small- and large-scale research programs. Uncertainties affecting aerodynamic performance that are associated with special configuration features resulting from the V/STOL requirement are addressed. Example uncertainties relate to minimum drag, wave drag, high angle-of-attack characteristics, and power induced effects.

| 17. Key Words (Suggested by Author(s)) | 18. Distribution Statement |
|---|---|
| V/STOL fighters; Powered lift; V/STOL aerodynamics; Vectored thrust; Top inlets; Propulsion simulators; Ejectors | Unlimited<br><br>Subject Category – 02 |

| 19. Security Classif. (of this report) Unclassified | 20. Security Classif. (of this page) Unclassified | 21. No. of Pages 38 | 22. Price* A03 |
|---|---|---|---|